Inorganic Chemistry

Viewpoint

pubs.acs.org/IC

Evaluation of Homogeneous Electrocatalysts by Cyclic Voltammetry

Eric S. Rountree, Brian D. McCarthy, Thomas T. Eisenhart, and Jillian L. Dempsey*

Department of Chemistry, University of North Carolina, Chapel Hill, North Carolina 27599-3290, United States

ABSTRACT: The pursuit of solar fuels has motivated extensive research on molecular electrocatalysts capable of evolving hydrogen from protic solutions, reducing CO_2, and oxidizing water. Determining accurate figures of merit for these catalysts requires the careful and appropriate application of electroanalytical techniques. This Viewpoint first briefly presents the fundamentals of cyclic voltammetry and highlights practical experimental considerations before focusing on the application of cyclic voltammetry for the characterization of electrocatalysts. Key metrics for comparing catalysts, including the overpotential (η), potential for catalysis (E_{cat}), observed rate constant (k_{obs}), and potential-dependent turnover frequency, are discussed. The cyclic voltammetric responses for a general electrocatalytic one-electron reduction of a substrate are presented along with methods to extract figures of merit from these data. The extension of this analysis to more complex electrocatalytic schemes, such as those responsible for H_2 evolution and CO_2 reduction, is then discussed.

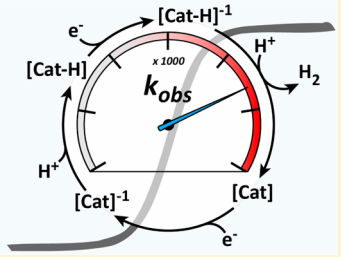

1. INTRODUCTION

The search to redefine humanity's energy portfolio has motivated researchers to seek inspiration for energy conversion schemes from nature, such as the elegant sunlight-to-fuel process of photosynthesis. Hydrogenase enzymes—with their ability to induce the oxidation of hydrogen or the reduction of protons to hydrogen—are an excellent example of fuel-forming catalysis in nature because hydrogen is a clean-burning, desirable fuel.[1] The intricate structures of hydrogenase enzymes contain inorganic active sites. This has motivated inorganic chemists to emulate the structure and activity of hydrogenases with the goal of creating synthetic catalysts capable of producing hydrogen from electron and proton feedstocks.[2−5] Studies of these small molecules have also aided in the fundamental understanding of enzyme mechanism and provide a platform with which to probe structure−function relationships. In parallel, extensive work has focused on the development of molecular catalysts for the reduction of CO_2 to yield carbon-based liquid fuels or fuel precursors,[6,7] as well as water oxidation, an essential half-reaction to pair with these reductive processes.[8,9] While it has yet to be determined if molecular inorganic catalysts are feasible on the scale required for global energy solutions,[10,11] these complexes could be an integral component in a sustainable energy approach to chemical fuel production if coupled with a renewable energy source, such as sunlight or wind.[12,13]

In part due to this recent escalation of research efforts directed toward the development of sustainable energy, the past decade has witnessed a dramatic resurgence in the use of electroanalytical methods by inorganic chemists.[2−4] While the protons and electrons for catalytic hydrogen production and CO_2 reduction eventually need to come from water, catalysts are usually evaluated in half-cell reaction schemes, where electrons are supplied by an electrode and protons by an acid. Consequently, researchers have turned to electrochemistry to evaluate catalysts for fuel production. Ideally, electrochemical techniques can be used to determine catalytic rate constants, afford information regarding the active catalyst identity, and help probe the mechanism. However, there exists a general lack of consensus in the community on how to accurately and appropriately extract figures of merit from electrochemical data. Some methods rely on assumptions which are not always carefully considered and can therefore result in misinterpretation of the collected data.

This Viewpoint is written for the researcher who seeks to use cyclic voltammetry (CV) to evaluate molecular catalysts. We primarily choose examples from the electrocatalytic hydrogen evolution literature to contextualize our discussion, but the tools presented can be directly extended to other reactions, including CO_2 reduction, hydrogen oxidation, water oxidation, and oxygen reduction. Fundamental concepts of CV are introduced alongside general experimental techniques before specific equations and concepts relevant to molecular electrocatalysis are described. Emphasis is placed on defining and discussing figures of merit within the scope of homogeneous catalysis.

2. ELECTROCHEMICAL METHODS

CV is the most commonly employed electroanalytical technique for studying molecular electrocatalysts. In this section, we briefly discuss the technique of CV before presenting practical experimental considerations. For a more thorough treatment on the fundamentals of CV, the reader is directed to the many excellent resources available in the literature.[14−19]

2.1. Cyclic Voltammetry. Illustrated in Figure 1 is a typical cyclic voltammogram for a solution-phase species P undergoing a reversible one-electron reduction to species Q. Starting at an initial potential at which the complex exists nominally in a

Received: March 21, 2014
Published: September 23, 2014

   dx.doi.org/10.1021/ic500658x | Inorg. Chem. 2014, 53, 9983−10002

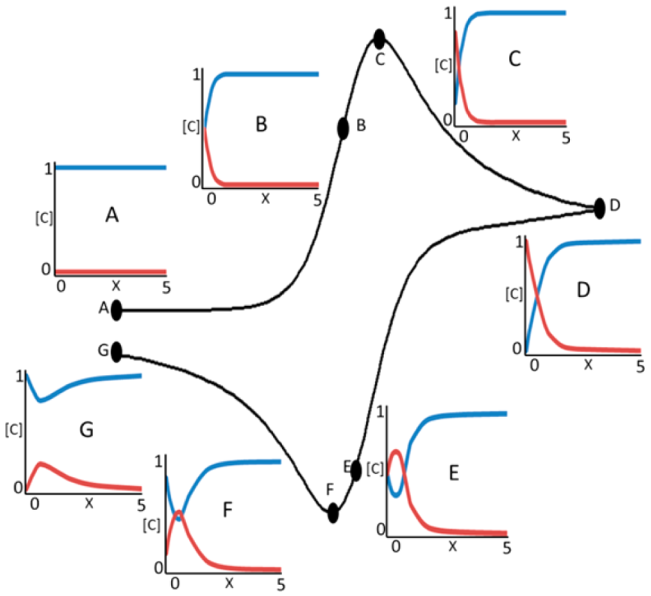

Figure 1. Concentration ([C], mM) versus distance from the electrode (x, cm × 10^{-2}) at various points during a reversible CV wave: C_P (blue); C_Q (red). Scan rate = 100 mV s^{-1}. Adapted from ref 16. Copyright 2011 Imperial College Press.

single redox state, P, the potential is scanned in the negative direction. When the potential is sufficiently negative to reduce P, a cathodic current begins to flow as P is reduced to Q. The current response is defined by the relationship of two parameters: the electron transfer rate constant between the electrode and analyte (k_C, proportional to k°, the standard heterogeneous electrochemical rate constant, an intrinsic property of the electrode–analyte pair under study, typically given in units of cm s^{-1}) and the transport (via diffusion) of the electroactive material to the electrode surface (described by the mass-transport coefficient, m_T).[15,16] When electron transfer to the analyte is rapid in relation to mass transport of the analyte ($k^\circ \gg m_T$, electrochemical reversibility) and the electrogenerated product is stable on the timescale of the experiment (chemical reversibility),[4] the rising cathodic current observed can be explained by the Nernst equation, shown below (eq 1) for the reaction P + e^- ⇌ Q, where C_P and C_Q are the concentrations of P and Q at the surface of the electrode, respectively, and $E^{\circ\prime}$ is the formal potential of the reduction process.[14]

$$E = E^{\circ\prime} + \frac{RT}{nF} \ln \frac{C_P}{C_Q} \quad (1)$$

When the applied potential is altered, the ratio of C_P and C_Q will adjust in accordance with the Nernst equation. In the limit of fast electrode kinetics, a dramatic increase in the cathodic current is observed at potentials in the region of $E^{\circ\prime}$ as P is reduced.

One might assume that the current should increase exponentially at even more negative potentials, as predicted by Butler–Volmer theory.[20] In fact, at sufficiently negative applied potentials, any oxidized species at the electrode surface is reduced, causing the concentration of the oxidized species (C_P) near the electrode (within the diffusion layer) to be diminished, as illustrated by the concentration–distance profiles shown in Figure 1. This effect is manifested in the voltammogram as a peak in the current (i_p) followed by a decrease in the current flow as the potential is scanned further negative. A concentration gradient is formed and the oxidized species from solution must be transported from the bulk solution to the electrode surface in order for additional current to flow. When high concentrations of the electrolyte and unstirred solutions are employed in CV experiments, diffusion can be well approximated as the sole mode of mass transport for the analyte and the rate of diffusion through the depleted diffusion zone dictates the observed current. The thickness of the diffusion layer (δ) depends on the timescale (t) of the voltammogram scan [$\delta \sim (Dt)^{1/2}$, where D is the diffusion coefficient of P, cm^2 s^{-1}], and t is inversely proportional to the scan rate υ ($t \sim RT/F\upsilon$).[20] As such, the diffusion layer thickens over the course of one scan, with the relative thickness decreasing with increasing scan rate.

At the switching potential, the scan direction is reversed, but the current continues to flow, as the applied potential is still sufficiently negative to reduce P, although the concentration of this species at the electrode has been significantly diminished by this point and the diffusion layer thickness has increased. Importantly, the depletion of P is matched by the accumulation of Q. As the applied potential becomes increasingly positive, Q is oxidized (such that the ratio of C_P/C_Q at the electrode surface satisfies the Nernst equation) and an anodic current flows following the same principles as described for the cathodic current.

2.2. Experimental Considerations. Moving from theory to practice, we first examine the experimental conditions under which electrocatalytic measurements are performed. Below we discuss each component of an electrochemical experiment and point out details to be conscious of and general practices to adhere to.

2.2.1. Solvent Choice. While water is the ultimate desired feedstock and solvent for solar fuel production schemes, many molecular electrocatalysts are studied in organic solvents. Most often, the choice of solvent is dictated by the solubility and stability of the catalyst.[18] The solvent influences several experimental considerations, including the electrolyte, reference electrode, and proton source (for catalytic H_2 generation and CO_2 reduction).

Electrochemical windows are defined by the potentials at which a given system begins to exhibit a current response not associated with the catalyst. The solvent, choice of electrolyte, working electrode, and substrate all affect the limits within which experiments can be performed. First, the redox properties of the solvent dictate the potential window. In water, for example, the negative end of the potential window is defined by the reduction of water to hydrogen at the electrode surface, while the positive end is defined by the oxidation of water for most electrodes. In nonaqueous systems, what occurs at the potential window terminals varies from solvent to solvent, but the window can still be defined by the potential at which the current flows beyond that seen for double-layer charging.[18] Second, the electrolyte can also have redox events, which limit the window, although this is rarely a large effect because common electrolytes are selected in part for their relatively inert nature. Third, the choice of working electrode will dictate the width of the potential window. Last, the direct reduction of protons (see section 2.2.3) at the electrode also limits the useful working range when certain forms of catalysis are carried out.

The use of low-conductivity solvents (e.g., organic solvents like acetonitrile and dichloromethane) may lead to large errors

dx.doi.org/10.1021/ic500658x | Inorg. Chem. 2014, 53, 9983–10002

in the measured potential as a result of uncompensated resistance; this is referred to as ohmic drop. Each solvent/electrolyte system has a unique solution resistance R_u, which induces a drop in potential (E_{OD}). Consequently, the potential at the electrode surface is given by $E_{actual} = E_{measured} - E_{OD}$.[21] The magnitude of E_{OD} can change dynamically during an experiment depending on the measured current, and this error can be estimated using Ohm's law: $E_{OD} = i_{measured}R_u$. Cathodic (negative) currents result in measured potentials that are falsely too negative, while anodic (positive) currents result in measured potentials that are falsely too positive.

The ohmic drop can be reduced in three ways: (1) positioning the reference electrode tip very near the surface of the working electrode using a Luggin capillary; (2) decreasing the size of the working electrode so that less current is passed; (3) increasing the conductivity of the solvent with higher concentrations of electrolyte. We have used chronoamperometry as a means of estimating the solution resistance for acetonitrile/electrolyte solutions.[22] Once the ohmic drop has been reduced in the experiment setup, the remaining ohmic drop error can be partially corrected for using active positive feedback, available in some commercial and custom-built potentiostats. Alternatively, the ohmic drop can be approximately corrected for after data collection, if the solution resistance is known, using Ohm's law.[22]

2.2.2. Reference Electrodes. Several reference electrodes are commonly used in aqueous electrochemical measurements; examples include the saturated calomel electrode (SCE), standard hydrogen electrode (SHE),[23] and the silver/silver chloride electrode (Ag/AgCl). Of note, the Ag/AgCl reference electrode can be prepared with various electrolyte compositions and concentrations that define the electrode potential, although saturated KCl is most common. However, for nonaqueous measurements, the primary choice of the reference electrode has not been standardized, in part because there is no universally reliable reference electrode.[18] The use of an aqueous reference electrode for nonaqueous measurements introduces an undefined, variable, and unmeasurable liquid junction potential to the cell, which is influenced by both the solvent and ionic strength.[18,24] Contamination of a nonaqueous solvent solution by water is another concern. Furthermore, the potentials measured in different solvents are not directly comparable, so it is uninformative to reference to an aqueous electrode when measurements are made in an organic solvent.

For acetonitrile and other nonaqueous solvents, a Ag/Ag^+ nonaqueous reference electrode represents the most stable choice (Box 1).[16,18] However, the potential of nonaqueous reference electrodes can vary between experiments due to variations in the Ag^+ concentration, electrolyte, or solvent. Care must also be taken when comparing data in the literature referenced to a Ag/Ag^+ electrode because the use of different reference electrode compositions (electrolyte identity, concentrations, etc.) leads to inconsistently reported redox potentials. Thus, as recommended by IUPAC, redox potentials measured using a nonaqueous reference electrode should be referenced by using an *internal reference* compound, specifically ferrocene (Fc), bis(biphenyl)chromium(0) (BCr), or an analogous redox couple that is known relative to that for Fc.[25,26] The Fc^+/Fc and BCr^+/BCr redox couples are well-defined and consistent in nonaqueous conditions and can be added directly to the analyte solution before or after analysis of the complex of interest. Conversion scales are available, but referencing the potential to the Fc^+/Fc couple (V vs Fc^+/Fc) is preferred.[24,27]

Box 1. Constructing reference electrodes

Glass electrodes can be constructed by attaching Vycor/CoralPor porous glass to glass tubes via heat-shrink tubing (see schematic at right). After attaching the tip, fill the glass tube with electrolyte solution and immerse the bottom of the tube in electrolyte. Allow to sit for several hours. Tap the glass If you notice bubble formation on the top of the porous glass tip. Store the tube in this state in a sealed container to prevent the porous glass from drying out. To prepare the reference electrode for use, remove the electrolyte solution from the glass tube and refill with the reference solution (see below). A well defined chemical internal standard (e.g., ferrocene) should be added at the end of each set of measurements to serve as a more reliable reference.

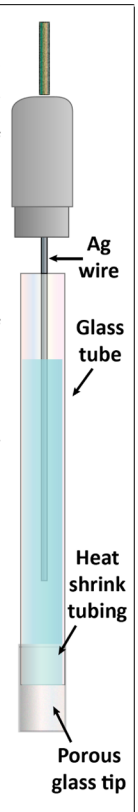

Saturated Ag/AgCl aqueous

Prepare the silver wire by dipping in 0.1 M HNO_3 to remove surface oxides, rinse with DI water, and immerse in bleach for thirty minutes to form a grayish coating of AgCl (under light color will darken). Rinse in DI water. Fill the reference electrode with saturated aqueous chloride salt (e.g., 4 M KCl) and insert the AgCl-coated silver into the tube. Store the AgCl wire in the dark when not in use.

$Ag/AgNO_3$ non-aqueous

Replace the electrolyte in the glass tube with a 0.01 M $AgNO_3$ solution containing the same electrolyte to be used in the experiment. Place a clean silver wire into the tube. Between experiments, the $AgNO_3$ solution should be removed and Ag free electrolyte added. Store $AgNO_3$ solutions in the dark.

Ag wire non-aqueous pseudoreference

Fill the glass tube with the same non-aqueous electrolyte solution as used in the experiment. Insert a bare Ag wire.

The $Ag/AgNO_3$ reference electrode is a commonly employed Ag/Ag^+ nonaqueous reference electrode. The preparation of a selection of reference electrodes including the $Ag/AgNO_3$ electrode is described in Box 1. A clean silver surface can be obtained by lightly polishing with 600 grit sandpaper or with a 2 s dip in 0.1 M HNO_3, followed by rinses with deionized water and acetone. The silver wire is inserted into a reference electrode body, which is constructed from a glass tube with a Vycor (Corning), CoralPor (Schott Glass), or porous Teflon tip. Extreme caution should be taken to avoid contamination from Ag^+ via leakage in a $AgNO_3$ reference electrode; leached Ag^+ may serve to augment the activity of the native electrode for H_2 evolution (electrodeposited Ag^0 on a glassy carbon electrode can be detected by the irreversible reduction of Ag^I at ca. −0.53 and −0.77 V as well as an irreversible oxidation of Ag^0 at ca. −0.14 V vs Fc^+/Fc in acetonitrile, as measured in our laboratory).[22]

A pseudoreference can also be utilized as a reference electrode. A pseudoreference electrode is a poorly defined reference, consisting of a metal wire such as platinum, silver, or gold. While the pseudoreference avoids the leakage issues seen in $Ag/AgNO_3$ reference electrodes, the reference potential of a pseudoreference electrode is ill-defined and is dependent on the composition of the electrolyte solution. Redox potentials measured using a pseudoreference electrode can be referenced to an internal reference compound, such as Fc. While the pseudoreference electrode can be immersed directly in the analyte solution, it is imperative to isolate the pseudoreference electrode in a fritted compartment during measurements wherein the sample composition varies over the course of an experiment, such as catalytic H_2 generation experiments involving the titration of acid between measurements. If the electrode is not isolated, the internal reference (e.g., Fc) must be present for each individual measurement (not added after

dx.doi.org/10.1021/ic500658x | *Inorg. Chem.* 2014, 53, 9983−10002

the measurements) such that any change in the potential can be corrected for and the experimenter must be aware of any reactivity of the pseudoreference electrode with species present in the solution or passivation of the pseudoreference electrode. Specifically, backgrounds of the internal reference with the substrate and electrolyte only (no catalyst) should be obtained. Last, the experimenter should also check that the internal reference in no way affects their measurement. This can be confirmed by performing a scan prior to the addition of the reference and one after to illustrate reproducibility of the data of interest.

2.2.3. Proton Sources. The choice of the proton source for catalytic H_2 evolution and CO_2 reduction is an important consideration. Several factors must be considered: catalyst stability and reactivity, direct reduction of acid at the electrode surface, and the influence of water on proton sources under otherwise nonaqueous conditions.

Catalyst reactivity with proton sources is dictated by both thermodynamic and kinetic parameters. Importantly, a catalyst cannot reduce an acid to hydrogen at potentials positive of the thermodynamic potential for reduction. In aqueous solution, the thermodynamic potential for H_2 evolution is defined as 0 V vs SHE and varies by −59 mV per pH unit with increasing pH per the Nernst equation. In nonaqueous solution, the thermodynamic potential for H_2 evolution depends on the acid and solvent identity, acid homoconjugation, and acid concentration. The thermodynamic potential for H_2 evolution from a given proton source (acid) must be determined for the precise experimental conditions employed, as is discussed in more detail in section 3.3.1.1.[28,29] Additionally, the observed acidity, and thus thermodynamic reduction potential, of a molecule is influenced by various processes, such as homoconjugation, heteroconjugation, and selective solvation.[30−32] The extent of this influence is dictated by the nature and concentration of the acid, and the solvent employed, factors that all must be considered for the selection of experimental parameters.[18,31]

The possibility of direct proton reduction at the working electrode must be considered in all experiments (Figure 2).[22,28] The potential at which the working electrode reduces protons

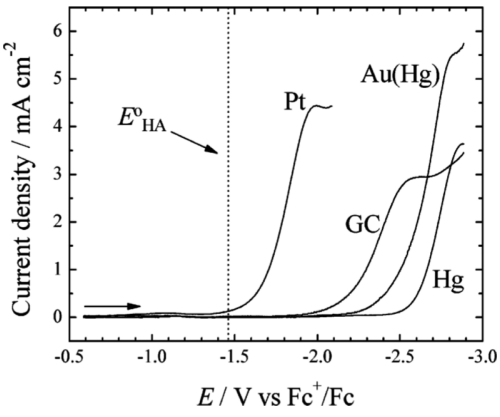

Figure 2. Linear-sweep voltammograms for 10 mM acetic acid in acetonitrile with 0.10 M tetrabutylammonium hexafluorophosphate at 1.0 V s^{-1}. Electrodes are as indicated [GC is glassy carbon, Au(Hg) is amalgamated gold]. Electrode areas differed; therefore, the current density is plotted. The reversible potential for the reduction of acetic acid is shown for comparison. Reprinted with permission from ref 28. Copyright 2006 American Chemical Society.

varies widely and depends on the proton source and electrode material. Platinum is a commonly employed working electrode for electroanalytical chemistry in general, but because of its exceptional ability to mediate H_2 evolution at relatively positive potentials in protic solutions, it is not considered a good choice for the study of electrocatalytic reactions.[28] Mercury electrodes give the largest window for electrocatalysis experiments with added acid, but safety, cost, and ease of use has led most researchers to employ glassy carbon (GC) electrodes. Of note, it is essential to polish the working electrode between every scan (and not just once prior to the first scan) because electrode surface fouling can result in erroneous values and irreproducibility.[22] Additionally, it should be noted that the GC material may vary by source and manufacturer.

When these first two factors are considered together, the potential range for a specific acid can then be considered to lie between the thermodynamic potential for proton reduction and the potential at which the electrode directly reduces the acid.[22] Electrocatalysis of interest should occur within this range. We recently reported the approximate acid potential windows in acetonitrile for 20 acids.[22] From a practical standpoint, one should define a potential window of reliability for experimental conditions by independently measuring the direct reduction of the substrate (e.g., acid, CO_2) by the working electrode, and this should be reported along with the data to avoid faulty or misleading performance for individual catalysts.[22,28]

It has recently been shown that many H_2 evolution catalysts originally studied under nonaqueous conditions show significantly enhanced catalytic response currents upon the addition of water.[33−36] Water may influence catalytic responses in several ways. For example, trace water has been shown, both experimentally and computationally, to dramatically affect the relative acidities of many acids in nonaqueous solvents. Charged species are usually selectively solvated by water, a process that is particularly effective for anionic conjugate bases with highly localized negative charge; the acidity in organic solvents, hence, is reported to increase with added water.[31,37] Additionally, solvation of anions through hydrogen bonding to water can overshadow nuanced differences between acids that influence the pK_a, like substituent effects.[18] On the other hand, the reduction of $HClO_4$ on a mercury electrode in acetonitrile has been shown to shift to more negative potentials upon the addition of water.[38] The observation was attributed to the large difference in the proton solvation energies between acetonitrile and water, with the former being much lower and resulting in the acid CH_3CNH^+, which is readily reduced in comparison to the weaker acid H_3O^+.

Water can also influence the mechanism of catalysis: water may act as a proton relay, donating a proton to the active site while accepting a proton from an outer sphere acid, with the small size of water consequently permitting increased access to sterically crowded active sites.[34] The shift in the pK_a upon the addition of water may lower the thermodynamic potential of direct acid reduction at the electrode, possibly resulting in a significant current contribution from this undesirable process in the same potential range as the catalytic reduction current. Last, concentrations of adventitious water may vary from sample to sample, posing problems for experimental reproducibility. The impact of water—whether intentionally added or adventitious—on electrocatalysis underscores the need to perform experiments in rigorously dry organic solvents, to identify possible sources of water contamination, and/or to quantify the

dx.doi.org/10.1021/ic500658x | *Inorg. Chem.* 2014, 53, 9983−10002

concentration of intentionally added water in nonaqueous experiments.

3. EVALUATING HOMOGENEOUS ELECTROCATALYSTS

Substantial growth in the field of molecular electrocatalysis has occurred over the past decade. Reports of electrocatalysts usually describe the catalytic activity with various metrics including overpotential, observed rate constants, turnover frequency (TOF), and Faradaic efficiency. Direct comparison between systems is difficult because the proton source, electrolyte, solvent, working electrode, and reference electrode almost always vary between reports. In addition, methods to determine metrics differ somewhat dramatically between laboratories. In this section, concise definitions of these metrics and benchmarks are first provided (section 3.1), followed by a short summary of the theoretical CV responses for an idealized E_rC_i' catalytic reaction (section 3.2) and detailed descriptions of the methods by which these metrics are obtained (section 3.3) and concluded by illustrative examples (section 3.4). Here we focus on determining parameters directly from CV, emphasizing the conditions that must be met to extract meaningful metrics. Metrics from rotating disk electrode methods, while powerful, are not discussed here in the interest of brevity, and the reader is directed to the literature.[39,40]

3.1. Key Definitions and Benchmarks. (i) The overpotential (η) is a thermodynamic parameter describing the additional potential, beyond the thermodynamic requirement, needed to drive a reaction at a *specific rate*.[20] It is defined as the difference between the applied potential and the standard potential for the formation of product B from substrate A ($E^\circ_{A/B}$). A detailed discussion of the overpotential is presented in section 3.3.1.1.

(ii) The standard potential for the catalysis-initiating redox couple (E_{redox}) defines the potential for the redox couple at which catalytic turnover occurs.

(iii) The half-wave potential ($E_{cat/2}$) is generally defined as the point at which the homogeneous catalytic wave reaches half of its maximum current. Because of complications with this notion when considering homolytic processes, a more encompassing description that we will adhere to is the potential at which half of the catalyst in the immediate vicinity of the electrode exists in the activated state.

(iv) The observed (or apparent) rate constant (k_{obs}) describes the overall rate of homogeneous catalysis. k_{obs} is useful for elucidating the reaction mechanism. In some works, this parameter has been termed TOF_{max}.[41] Depending on the complexity of the reaction and the specific conditions, k_{obs} can be interpreted to consist of a single rate-limiting step (such as protonation or reductive elimination of the product) or to be a rate expression composed of rate constants for individual steps of catalysis. Methods to evaluate k_{obs} are discussed in sections 3.3.2.1−4.

(v) The TOF is a kinetic parameter that quantifies the catalytic activity (section 3.3.2.5). Specifically, TOF is the number of moles of product (e.g., H_2, O_2, CO, CH_2O) evolved per unit of time per mole of catalyst. Importantly, for homogeneous molecular catalysis, TOF describes the activity of the catalyst molecules contained in the reaction−diffusion layer at the electrode, not the catalyst molecules contained in the whole bulk solution. Because TOF depends on the percentage of catalyst molecules activated (a potential-dependent parameter), TOF only equals k_{obs}(TOF_{max}) when the applied potential is sufficiently negative (or positive) of the redox couple such that effectively 100% of the catalyst is in the active form.

(vi) TOF_0 is the extrapolated TOF at $E = E^\circ_{A/B}$.[42] The theoretical TOF_0 is proposed elsewhere[42] as an "intrinsic" TOF for the catalyst (section 3.3.2.5).

3.2. E_rC_i' Catalytic Mechanism and Idealized CV Responses. Electrocatalytic processes, like H_2 evolution and CO_2 reduction, can occur via many mechanisms with numerous possible CV responses. These responses may be dependent on multiple variables including the scan rate, catalyst and substrate concentrations, and rate constants of the catalytic mechanism. Correct modeling of the CV response for a specific catalyst, and consequently accurate determination of the rate constant, requires that the mechanism be known. Savéant and co-workers have rigorously mapped out the various CV responses for the one-electron reduction of substrate A to B by a redox catalyst P, where the rate-limiting step is homogeneous electron transfer (the E_rC_i' mechanism).[44,45]

$$P + e^- \rightleftharpoons Q$$

$$Q + A \xrightarrow{k_e} P + B$$

The CV responses for this process depend on the parameters[44]

$$\lambda = \left(\frac{RT}{F}\right)\left(\frac{k_e C_P^0}{\upsilon}\right)$$

$$\gamma = \frac{C_A^0}{C_P^0}$$

where λ is the kinetic parameter, γ is the excess factor, k_e is the rate constant of outer-sphere electron transfer from the reduced catalyst Q to substrate A, C_P^0 is the bulk concentration of redox catalyst P, and C_A^0 is the bulk concentration of substrate A. A two-dimensional plot of λ versus γ can be created and the various limiting CV responses divided into zones (Figure 3).[43,44] While this zone diagram specifically models one-electron redox catalysis with homogeneous electron transfer as the rate-determining step, the various regions and CV responses have become general reference points for more complicated mechanisms.[46] Additionally, commonly used equations for determining the apparent rate constants (see section 3.3.2) for electrocatalysts originate from this analysis. Consequently, the various zones and CV responses from Figure 3 are discussed here, as well as how different zones may be accessed by varying λ and γ, as suggested by the compass rose in the figure.

Zone D (No Catalysis). The CV observed is that of the reversible redox couple P/Q.

Zone KS (S-Shaped, Pure Kinetic Conditions,[44] No Substrate Consumption). In zone KS, an S-shaped response is observed where the forward and reverse scans trace each other exactly. This region is characterized by the situation where the substrate concentration at the electrode surface is equal to the bulk concentration. Accessing this region from zone K (see below) consequently hinges on avoiding substrate depletion at the electrode and, as suggested in the compass rose of Figure 3, can been accessed by increasing the scan rate (consequently decreasing λ) such that the total time required to record the CV—the time when the substrate is being depleted—is short.[47]

dx.doi.org/10.1021/ic500658x | Inorg. Chem. 2014, 53, 9983−10002

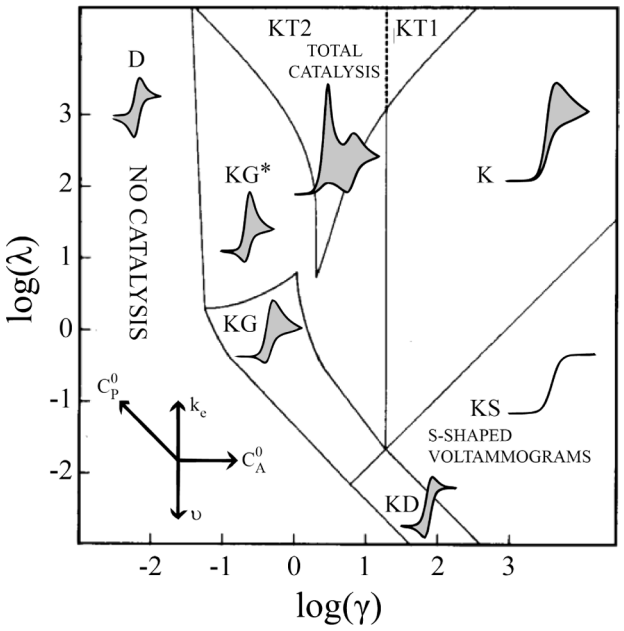

Figure 3. Kinetic zone diagram and simulated CV waveforms for the one-electron reduction of substrate A via redox catalyst mediator P, where λ is the kinetic parameter and γ is the excess factor (see the text). The compass rose visually depicts how catalysis may move between zones (C_P^0 is the initial concentration of the catalyst, C_A^0 is the initial concentration of the substrate, υ is the scan rate, and k_e is the rate constant for homogeneous electron transfer from the reduced catalyst to the substrate). The CV waveforms follow the convention of negative potentials to the right and cathodic current upward. Scans are started from positive potentials. Waveforms are adapted with permission from ref 43. Copyright 2008 American Chemical Society. The zone diagram is reprinted (with minor modifications) with permission from ref 44. Copyright 1984 Elsevier.

Zone K (Pure Kinetic Conditions, Substrate Consumption). In zone K, competition between consumption of the substrate by the rate-determining step, with diffusion of a new substrate to the electrode, results in a peaked CV and a reverse scan that does not lie on top of the forward scan. Despite depletion of the substrate, no reverse redox wave is seen because any reduced catalyst is oxidized through catalytic turnover.

Zone KT2 (Total Catalysis, Pure Kinetic Conditions, Substrate Consumption). Total catalysis is observed when the catalyst immediately consumes all of the accessible substrate within the timescale of the forward scan, resulting in a CV with two peaks. A catalytic current is initially observed, but the substrate is quickly totally consumed, resulting in a peak. As the potential is scanned more negative, the reversible redox wave of the catalyst is seen in the same position without substrate present.

Zone KT1 (Pure Kinetic Conditions, Substrate Consumption). A catalyst may move from zone KT2 to zone KT1 as the excess factor γ increases. With increasing γ, the reversible wave becomes buried under the catalytic wave, erasing the distinction of two separate peaks. Increasing γ further pushes the CV response into zone K. Zones KT1 and KT2 are special cases of the pure kinetic zone K.[44]

Zone KD (No Substrate Consumption). The waveform depicted in zone KD describes catalysts that are operating under the conditions of no substrate consumption (large γ), similar to that of zone KS. However, in this scenario the waveform is not a perfect "S" shape because of a reduced value of the kinetic parameter, λ. A catalyst can potentially move from zone KS to zone KD by increasing the scan rate of a CV experiment, effectively outcompeting the rate at which a catalyst turns over. Catalysts that have slower rate constants than those in zone KS will also give waveforms similar to those found in zone KD. Using the plateau current of the waveform in zone KD, a catalytic rate constant can be determined using eq 10 (see below).[45]

Zones KG and KG (Substrate Consumption).* Waveforms depicted in zones KG and KG* arise from conditions described by small γ and λ.[44] Similar to zone KT2, where total catalysis occurs, zones KG and KG* are limited by substrate diffusion to the electrode from the bulk. In this case, the dimensionless kinetic parameter for waveforms in these zones is also small, meaning one can move from zone KT2 to zone KG/KG* by using a catalyst with slower kinetics or increasing the scan rate used in analysis. One can also move from the KD region to KG/KG* by lowering the substrate concentration or increasing the catalyst concentration to decrease γ.

Extension to More Complicated Mechanisms. This waveform discussion has focused on the specific example of a one-electron catalytic process by which electron transfer to substrate A occurs via an outer-sphere mechanism. While the electrocatalytic reactions of interest here occur via more complicated mechanisms (see below), the waveforms presented in Figure 3 are relatively general because the concepts of the catalytic rate and substrate diffusion are generally applicable across various molecular electrocatalytic systems. For example, it has been demonstrated for electrochemical H_2 evolution catalysts that different zones can be accessed by varying the scan rate.[47] A more quantitative discussion on these catalytic regimes follows.

3.3. Determining Figures of Merit from CV. *3.3.1. Thermodynamic Parameters: Overpotential and Potential for Catalysis. 3.3.1.1. Overpotential (η).* The overpotential (η) represents the driving force of a reaction and is defined as the additional potential, beyond the thermodynamic requirement, needed to drive a reaction at a *specific rate*.[20] This thermodynamic parameter is calculated as the difference between the applied potential and the standard potential for the formation of product B from substrate A ($E^\circ_{A/B}$; eq 2).

$$\eta = E - E^\circ_{A/B} \tag{2}$$

$E^\circ_{A/B}$ must be independently evaluated in order to determine η. Returning to the example of H_2-evolving catalysts, we highlight that the thermodynamic potential for H_2 evolution (E°_{HA/H_2} and $E^\circ_{H_2O/H_2}$) is specific to a given acid source, its concentration, and the solvent employed. In aqueous solution, the standard potential ($E^\circ_{H_2O/H_2}$) is defined by the SHE. At pH 0, hydrogen is evolved at 0 V vs SHE, and the thermodynamic potential shifts 59 mV with each pH unit. Determination of the thermodynamic potential for H_2 evolution in nonaqueous solvents (E°_{HA/H_2}) is substantially more challenging. E°_{HA/H_2} is proportional to the acid strength (defined by the acid dissociation constant of the acid in a specific nonaqueous solvent S, $pK_{a,HA,S}$), and for acids with $pK_{a,HA,S} > 0$, Evans has defined the relationship by eq 3, which is based on the Nernst equation:[28]

$$E^\circ_{HA/H_2} = E^\circ_{H^+/H_2} - \left(\frac{2.303RT}{F}\right)pK_{a,HA,S} \tag{3}$$

dx.doi.org/10.1021/ic500658x | Inorg. Chem. 2014, 53, 9983−10002

where $E^{\circ}_{H^+/H_2}$ is the standard potential for the solvated proton/dihydrogen couple. There is a disagreement between the reported values of $E^{\circ}_{H^+/H_2}$.[28−30,48,49] The most recently measured value for acetonitrile (−0.028 V vs Fc^+/Fc) is recommended based on the robustness of the open-circuit-potential (OCP) method (discussed below) used to determine this value.[29]

While eq 3 provides an *estimate* for E°_{HA/H_2}, Roberts and Bullock have recently reported a direct determination of E°_{HA/H_2} by OCP measurements.[29] This approach is ideal for cases wherein pK_a of a given acid or $E^{\circ}_{H^+/H_2}$ is unknown for a particular solvent or when homoconjugation effects must be taken into account.[50] In this measurement, a CV is recorded for an analyte solution consisting of an acid/base/hydrogen mixture and an internal reference (Fc), using a GC working electrode, a Ag/AgCl nonaqueous reference electrode, and a counter electrode. A potentiometer is used to measure the OCP between the reference electrode and a platinum wire electrode, in effect determining E°_{HA/H_2}. As noted above, this approach does not require independent values for $pK_{a,HA,S}$, homoconjugation constants, or $E^{\circ}_{H^+/H_2}$ and works in a wide range of acid/base and solvent systems. It was also noted that good agreement was found between the measured values and values calculated from known $pK_{a,HA,S}$ values using the Nernst equation.

Artero et al. have also challenged the use of eq 3, noting that the method does not account for the acid concentration.[30] Instead, they advocate a method to calculate the theoretical half-wave potential ($E^{T}_{1/2}$), which corresponds to the potential at which half of the maximum acid reduction current is obtained with an ideal electrode (eq 4; note correction of "=" typo from equation in original article), which can be used in place of E°_{HA/H_2}.[30]

$$E^{T}_{1/2,HA/H_2} = E^{\circ}_{H^+/H_2} - \left(\frac{2.303RT}{F}\right)pK_{a,HA,S} + \varepsilon_D - \frac{RT}{2F}\ln\frac{C_0}{C^0_{H_2}} \quad (4)$$

where C_0 is the total concentration of acid, ε_D is a measure of the relative diffusion of products versus reactants, and $C^0_{H_2}$ is the concentration of dissolved hydrogen corresponding to a partial pressure of 1 bar.[30] Additionally, related expressions are available[30] for conditions under which acids display homoconjugation by invoking equilibrium constants for aggregation reactions, as well as expressions for $E^{T}_{1/2}$ when A^- or H_2 are initially present in solution.

Like H_2, the standard potentials for O_2 reduction (and water oxidation) and CO_2 reduction are condition specific. The standard potential for the four-electron reduction of O_2 to water ($E^{\circ}_{O_2/H_2O}$) under the standard conditions (1 M aqueous acid, pH 0) is 1.229 V vs NHE, and like H_2, the thermodynamic potential shifts −59 mV per pH unit as the pH is increased. To our knowledge, the standard potential of this half-reaction has not been determined in nonaqueous media, but in the absence of calculations, it should be noted that $E^{\circ}_{O_2/H_2O}$ will be dependent on the proton source and solvent. The standard potential for the two-electron reduction of CO_2 to CO under standard aqueous conditions (1 M aqueous acid, pH 0) is −0.106 V vs NHE (and exhibits the same Nernstian dependence as H_2 and O_2 reduction). Other proton-coupled multielectron reductions of CO_2 and their corresponding thermodynamic potentials are summarized in Table 1.[51] The

Table 1. Potentials for CO_2 Reduction at pH 7, 25 °C, 1 atm of Gas Pressure, and 1 M for Other Solutes[6,52]

reaction	$E^{\circ\prime}$ (V vs NHE)
$CO_2 + 2H^+ + 2e^- \rightarrow CO + H_2O$	−0.53
$CO_2 + 2H^+ + 2e^- \rightarrow HCO_2H + H_2O$	−0.61
$CO_2 + 4H^+ + 4e^- \rightarrow HCHO + H_2O$	−0.48
$CO_2 + 6H^+ + 6e^- \rightarrow CH_3OH + H_2O$	−0.38
$CO_2 + 8H^+ + 8e^- \rightarrow CH_4 + 2H_2O$	−0.24
$CO_2 + e^- \rightarrow CO_2^{\bullet -}$	−1.90

thermodynamic potential for the two-electron reduction of CO_2 to CO in nonaqueous solvents [dimethylformamide (DMF), eq 5; acetonitrile, eq 6] in the presence of acids HA has recently been estimated by Costentin and Savéant, who utilized a detailed thermodynamic cycle that accounts for the free-energy changes associated with moving components from water to nonaqueous media.[42,51] To our knowledge, the same has not been calculated for the other multielectron reduction processes described in Table 1.

$$E^{\circ}_{CO_2/CO,DMF,HA} = -0.259 - \left(\frac{2.303RT}{F}\right)pK_{a,HA,DMF} \text{ V vs NHE} \quad (5)$$

$$E^{\circ}_{CO_2/CO,CH_3CN,HA} = 0.349 - \left(\frac{2.303RT}{F}\right)pK_{a,HA,CH_3CN} \text{ V vs NHE} \quad (6)$$

As underscored in the definition presented above, the overpotential is a key figure of merit when associated with a kinetic parameter; at what *rate* is catalysis being driven with applied potential E? Unfortunately, this metric is often used to evaluate molecular catalysts without reference to any kinetic parameter, creating ambiguity in its meaning. What is the best potential-dependent kinetic parameter to utilize when reporting overpotential? In heterogeneous electrochemistry, the current density is commonly reported, and the relationship between the current density and overpotential provides the classic Tafel plot. Per the Tafel equation, the catalytic current increases exponentially with increasing overpotential.[20] Molecular systems, however, behave in an entirely different manner.[50] Catalysis is "triggered" by a redox process, such as the reduction of catalyst P to species Q, which has a standard potential (which we refer to as E_{redox}; see sections 3.2 and 3.3.2). This redox event acts as an on−off switch for catalysis. The catalyst has an associated homogeneous apparent rate constant (k_{obs}) for turnover of the catalytic cycle, which is a property of the mechanism employed and generally not the applied potential (although it can be dependent on the solvent, acid strength, or temperature; in scenarios with two competing mechanisms activated at different potentials, k_{obs} will then be potential-dependent). As described in sections 3.3.2.1−4, in many, but not all, cases, k_{obs} can be determined from the plateau current, reached at potentials where the fraction of active catalyst (Q) is near unity, as described by the Nernst equation. By contrast, the TOF is a potential-dependent kinetic parameter that has a defined relationship with k_{obs} (which can be considered a TOF_{max}). The TOF−η relationship, as defined by Savéant and

dx.doi.org/10.1021/ic500658x | Inorg. Chem. 2014, 53, 9983−10002

Costentin, is discussed in detail in section 3.3.2.5.[41,42] In TOF−η analyses, the potential dependence of TOF in the region of a catalytic voltammogram prior to the current plateau reflects the subunity fraction of activated catalyst (Q). The Tafel-like plots produced from this relationship provide an opportunity for benchmarking the performance of molecular catalysts (under certain limits, as discussed below).

3.3.1.2. Catalysis-Initiating Redox Potential (E_{redox}), Half-Wave Potential ($E_{cat/2}$), and Potential Necessary for Catalysis (E_{cat}). Because of the difficulty of correlating the applied potential with kinetic data for molecular catalysts, a parameter to describe the "overpotential necessary for catalysis"—the difference between the potential necessary for catalysis (E_{cat}) and $E^{\circ}_{A/B}$—has been commonly utilized in the literature. For this discussion, we define this term as shown in eq 7 and differentiate it from η, which was defined in the previous section (eq 2).

$$\text{overpotential necessary for catalysis} = E_{cat} - E^{\circ}_{A/B} \tag{7}$$

Depending on how E_{cat} is determined (as discussed below), it is often just a rough estimate of the applied potential necessary for catalysis, although in idealized cases, E_{cat} can contain kinetic information.[41] As such, the value defined by eq 7 can be an imprecise figure of merit. For this reason, we distinguish this general term from the specific definition presented in eq 2 and reserve the term "overpotential" for catalyst parametrization when meaningful kinetic data are correlated with the applied potential, which is necessary for comparison.

In recent years, the definition of E_{cat} has been a very subjective notion and, as such, various methods to determine E_{cat} have been reported, including (1) the potential at which "onset" of the catalytic peak is seen, (2) the potential of the peak current, (3) the potential at which the electrocatalyst undergoes a mechanistically relevant redox process in the absence of substrate (E_{redox}), and (4) the potential at which half of the maximum current is obtained ($E_{cat/2}$; note that, at $E_{cat/2}$, half of the catalyst in the reaction−diffusion layer exists in the activated state; this broader definition accounts for the fact that, for a homolytic reaction mechanism, 50% of the catalyst is *not* activated when half of the maximum catalytic current is reached).[30] The lack of a standard method means that E_{cat} can differ by almost 200 mV,[30] yielding uncertainty among reports that employ different definitions. Method 1 is inherently subjective (what magnitude of current should count as the catalytic current?) and does not accurately describe the thermodynamic energy associated with the catalytic event. Method 2 is not applicable because well-defined peaks, when observed, give no information about the reaction itself because the peak potential depends on the extent of substrate depletion.[42]

For an E_rC_i' mechanism operating under ideal conditions in which the canonical S-shaped waves are observed, $E_{cat/2} = E_{redox}$, and thus methods 3 and 4 will give the same value.[41] For various two-electron, two-step catalytic mechanisms, the relationships of $E_{cat/2}$ and E_{redox} have been defined, as have the corresponding TOF−η expressions (see section 3.3.2).[41] However, when side phenomena preclude an S-shaped response (and a peak-shaped, scan-rate-dependent response is obtained), determining a meaningful and accurate $E_{cat/2}$ may be difficult or impossible. Perturbations of the substrate concentration and scan rate will lead to a change in $E_{cat/2}$. Appel and Helm[50] have suggested that the $E_{cat/2}$ potential determined for a nonideal catalytic wave will have only a small variance from the true $E_{cat/2}$, but we caution that kinetic information can only be loosely estimated from this approach, preventing benchmarking.

In summary, we caution that the overpotential necessary for catalysis, as has been reported in recent years, should not be considered a general parameter for direct, quantitative, catalyst comparison between independent reports because of the nonuniform use of the parameter E_{cat}. When they can be directly measured, E_{redox} and $E_{cat/2}$ both provide meaningful information, both for mechanistic analysis (see section 3.3.2.2) and for catalyst comparison. E_{redox} provides insight into the thermodynamics associated with the reaction, while $E_{cat/2}$ aids in the kinetic comparison from one catalyst to another through its part in the TOF−η relationship (see section 3.3.2). $E^{\circ}_{A/B}$ is specific to each solvent and proton source employed; using the example of H_2 generation, the overpotential necessary for catalysis can often be decreased by employing acids with more negative E°_{HA/H_2} values (weaker acids) if E_{redox} and/or $E_{cat/2}$ remain constant. However, when a series of catalysts are measured under the same conditions and the E_{cat} definition employed is clearly correlated with a kinetic parameter, the overpotential for catalysis can be utilized for catalyst comparison. Still, a complete TOF−η relationship will be more useful.

3.3.2. Kinetic Parameters: Observed Rate Constants and TOF. Determining kinetic and mechanistic information for molecular catalysts from CV can be a challenging endeavor, especially for multielectron, multistep reactions. In this section, methods for extracting the overall rate of catalysis are discussed in detail.

3.3.2.1. Determining a Rate Constant for a E_rC_i' Reaction from CV. Key reaction parameters, such as the apparent rate, can be determined directly from voltammograms of active catalysts. This section introduces the process for determining the apparent rate constant (k_{obs}) for a simple E_rC_i' mechanism, followed by a discussion of the approximations that allow figures of merit for more complex reactions like electrocatalytic H_2 generation and CO_2 reduction to be evaluated.

The theory behind the CV of catalytic E_rC_i' reactions was formulated by Delahay and Stiehl,[53] Nicholson and Shain,[54,55] and Savéant and co-workers.[44,56−59] The reaction of interest, introduced in section 3.2, is repeated here for clarity.

$$P + e^- \rightleftharpoons Q$$

$$Q + A \xrightarrow{k_e} P + B$$

Several assumptions are made: electron transfer between the electrode and redox-active couple P/Q is fast and Nernstian; by corollary, the homogeneous electron transfer (chemical) step (Q + A) that reforms P is rate-limiting; $C^0_A \gg C^0_P$ (large γ); the diffusion coefficients of species P and Q are approximately equal; E_i (the initial potential of the scan) is sufficiently positive such that the resulting measurement is independent of this value; substrate A exhibits no redox behavior at the electrode in the window of interest. The observed (or apparent) pseudo-first-order rate constant, k_{obs}, is defined by eq 8 (for the E_rC_i' mechanism) and is intrinsic to the homogeneous chemical reaction Q + A and hence not potential-dependent. Simply stated, k_{obs} represents the rate at which P is formed from Q through a homogeneous process.

$$k_{obs} = k_e C^0_A \tag{8}$$

dx.doi.org/10.1021/ic500658x | Inorg. Chem. 2014, 53, 9983−10002

Table 2. k_{obs} and $E_{1/2}$ Expressions for Several Two-Electron, Two-Step Reaction Pathways (Adapted from Reference 41)

Heterolytic Reaction Processes			
All electron transfers occur at the electrode* $i_c = 2FAC_P^0\sqrt{Dk_{obs}}$		**One homogeneous electron transfer** $i_c = FAC_P^0\sqrt{D2k_{obs}}$	
EECC			
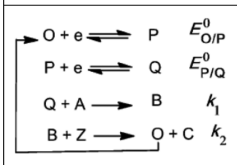	For $k_2C_Z^0 \gg k_1C_A^0$ $k_{obs} = k_1C_A^0$ $E_{cat/2} = E^o_{P/Q}$ For $k_2C_Z^0 \ll k_1C_A^0$ $k_{obs} = k_2C_Z^0$ $E_{cat/2} = E^o_{P/Q} + \frac{RT}{F} ln\left(\frac{\sqrt{k_1C_A^0}}{\sqrt{k_2C_Z^0}}\right)$	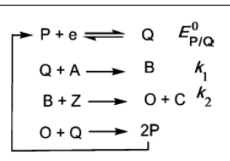	For $k_2C_Z^0 \gg k_1C_A^0$ $k_{obs} = k_1C_A^0$ $E_{cat/2} = E^o_{P/Q}$ For $k_2C_Z^0 \ll k_1C_A^0$ $k_{obs} = k_2C_Z^0$ $E_{cat/2} = E^o_{P/Q} - \frac{RT}{F} ln\left(\frac{\sqrt{2k_2C_Z^0}}{\sqrt{k_1C_A^0}}\right)$
ECEC, $E^o_{P/Q} < E^o_{Q\prime/B}$			
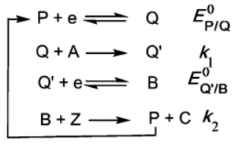	For $k_2C_Z^0 \gg k_1C_A^0$ $k_{obs} = k_1C_A^0$ $E_{cat/2} = E^o_{P/Q}$ For $k_2C_Z^0 \ll k_1C_A^0$ $k_{obs} = k_2C_Z^0$ $E_{cat/2} = E^o_{P/Q} + \frac{RT}{F} ln\left(\frac{\sqrt{k_1C_A^0}}{\sqrt{k_2C_Z^0}}\right)$	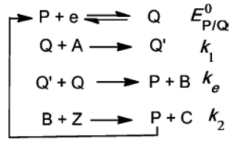	For $k_2C_Z^0 \gg k_1C_A^0$ $k_{obs} = k_1C_A^0$ $E_{cat/2} = E^o_{P/Q}$ For $k_2C_Z^0 \ll k_1C_A^0$ *To determine k_{obs}, treat as if ET occurs at electrode* $E_{cat/2} = E^o_{P/Q} + \frac{RT}{F} ln\left(\frac{\sqrt{k_1C_A^0}}{\sqrt{2k_2C_Z^0}}\right)$
ECCE, $E^o_{P/Q} < E^o_{Q\prime\prime/P}$			
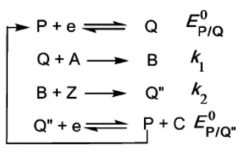	For $k_2C_Z^0 \gg k_1C_A^0$ $k_{obs} = k_1C_A^0$ $E_{cat/2} = E^o_{P/Q}$ For $k_2C_Z^0 \ll k_1C_A^0$ $k_{obs} = k_2C_Z^0$	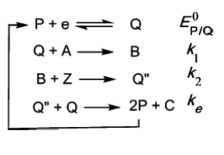	For $k_2C_Z^0 \gg k_1C_A^0$ $k_{obs} = k_1C_A^0$ $E_{cat/2} = E^o_{P/Q}$ For $k_2C_Z^0 \ll k_1C_A^0$ $k_{obs} = k_2C_Z^0$
	$E_{cat/2} = E^o_{P/Q} + \frac{RT}{F} ln\left(\frac{\sqrt{k_1C_A^0}}{\sqrt{k_2C_Z^0}}\right)$		$E_{cat/2} = E^o_{P/Q} - \frac{RT}{F} ln\left(\frac{\sqrt{2k_2C_Z^0}}{\sqrt{k_1C_A^0}}\right)$
ECCE, $E^o_{P/Q} > E^o_{Q\prime\prime/P}$ *electron transfer at electrode only, unfavorable homogeneous electron transfer pathway* Note: the second electron transfer process is a dissociative electron transfer reaction, as such it does not obey the Nernst law.[41] In this scenario, the Butler–Volmer law must be utilized, as such the rate constant k_S for the heterogeneous dissociative ET step and the transfer coefficient α have been incorporated into the equations below.			
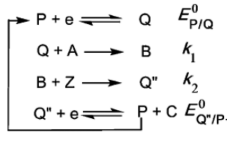	For $k_2C_Z^0 \gg k_1C_A^0$ $k_{obs} = k_1C_A^0$ $E_{cat/2} = \left(E^o_{Q''/P+C} + \frac{RT}{F\alpha}\ln k_S\right) - \frac{RT}{F\alpha}\ln\sqrt{Dk_1C_A^0}$	For $k_2C_Z^0 \ll k_1C_A^0$ $k_{obs} = k_2C_Z^0$ $E_{cat/2} = \left(E^o_{Q''/P+C} + \frac{RT}{F\alpha}\ln k_S\right) - \frac{RT}{F\alpha}\ln\sqrt{Dk_2C_Z^0}$	
ECEC, $E^o_{P/Q} > E^o_{Q\prime/B}$ *electron transfer at electrode only, unfavorable homogeneous electron transfer pathway* *the i_c equation introduced in the header is not applicable to this scenario			
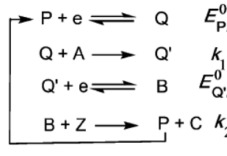	$i_c = 2FAC_P^0\sqrt{D}\frac{1}{\frac{1}{\sqrt{k_1C_A^0}} + \frac{1}{\sqrt{k_2C_Z^0}}}$ $E_{cat/2} = E^o_{Q\prime/B} + \frac{RT}{F} ln\left(1 + \frac{\sqrt{k_2C_Z^0}}{\sqrt{k_1C_A^0}}\right)$		

dx.doi.org/10.1021/ic500658x | *Inorg. Chem.* 2014, 53, 9983−10002

Table 2. continued

Homolytic Reaction Process *the i_c equation introduced in the header is not applicable to this scenario	
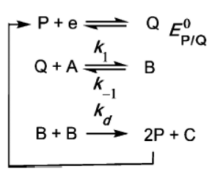	$i_c = FA\sqrt{\frac{4Dk_d}{3}}\frac{k_1 C_A^0}{k_{-1}}\frac{(C_{cat}^0)^{3/2}}{\left(1+\frac{k_1 C_A^0}{k_{-1}}\right)^{3/2}}$ $E_{cat/2} = E^o_{P/Q} + \frac{RT}{F} ln\left(1+\frac{k_1 C_A^0}{k_{-1}}\right)$

In the limiting case of large $\lambda/C_P^0 = k_{obs}RT/F\upsilon$ (which, together with the previously stated assumption of a large γ, indicates zone KS), the resulting wave can be described by eq 9, where n is the number of electrons transferred in the redox event, A the electrode surface area in cm^2 (usually treated as the geometric surface area, although the electrochemical surface area is preferred), D the diffusion coefficient of the redox species P in $cm^2\ s^{-1}$, and C_P^0 the bulk concentration of redox species P in mol cm^{-3}.

$$i = \frac{nFAC_P^0\sqrt{Dk_{obs}}}{1 + \exp\left[\frac{nF}{RT}(E - E^\circ_{P/Q})\right]} \quad (9)$$

Importantly, eq 9 indicates that no peak is observed. At potentials significantly negative of $E^\circ_{P/Q}$ (≈100 mV), eq 9 is simplified and the catalytic plateau current i_c can be described by eq 10. i_c is independent of the scan rate because the current is controlled only by regeneration of P through the chemical reaction Q + A.[58]

$$i_c = nFAC_P^0\sqrt{Dk_{obs}} \quad (10)$$

k_{obs} can be deduced from i_c. Frequently, the i_c–k_{obs} relationship is divided by the Randles–Sevcik equation (eq 11), which describes the dependence of the peak current i_p (amperes) on the scan rate υ (V s^{-1}) for a reversible redox process.

$$i_p = 0.4463nFAC_P^0\left(\frac{nF\upsilon D}{RT}\right)^{1/2} \quad (11)$$

This yields the relationship shown in eq 12.

$$\frac{i_c}{i_p} = \frac{1}{0.446}\sqrt{\left(\frac{RT}{nF\upsilon}\right)k_{obs}} \quad (12)$$

Equation 12 is often desirable because it does not require an independent measurement of D, A, or C_P^0 to determine k_{obs}. It must be noted that n in eq 10 represents the number of electrons transferred to P from the electrode and thus is only different from n in eq 11 in the case where i_p is determined from a separate redox event (this may at times be necessary because of some interference at the event of interest[47]) or when successive electron transfers occur at the electrode following chemical steps. This is discussed further in section 3.3.2.3, but it should be noted that, as written, eq 12 assumes that the value of n in eq 10 is 1.

It is worth reiterating that the use of eqs 10 and 12 is restricted to the S-shaped curves obtained in zones KS and KD (where the plateau current is used).[45] Access to zone KS (and KD) necessitates that i_c is not limited by substrate diffusion; substrate consumption is always negligible so that the assumption $C_A = C_A^0$ holds true. Experimentally, the S-shaped CV response of zone KS can be obtained by increasing the substrate concentration (increasing γ) or increasing the scan rate to limit substrate consumption. Additionally, access to the pure kinetic zones requires the chemical reaction be fast in comparison to the timescale of the voltammogram; thus, in the case of slow catalysis (small k_e), υ may be decreased to increase the value of λ. However, caution must be exercised because slow scan rates (and very large λ) may lead to substrate consumption within the diffusion layer. To ensure that an appropriate scan rate is being utilized, the scan rate independence of i_c should be confirmed.[33] Further, at very slow scan rates, a "false" plateau shape may be achieved as a result of natural convection.[7,58] Last, in many cases, the S-shaped response wave may not be accessible. Side phenomena, such as catalyst deactivation, inhibition of the current by product adsorption to the electrode, and background H_2 evolution, are known to perturb catalytic responses.[42]

To this point, eqs 10 and 12 have been discussed in the case where the observed rate, k_{obs}, is simply equal to $k_eC_A^0$. However, these equations have been used extensively to estimate the catalytic rates of more complex systems, in particular the electrocatalytic generation of H_2. In these systems, k_{obs}, the global rate constant, describes the overall observed rate of catalyst turnover (see below). Proper extension of E_rC_i' theory to these more complex catalytic systems requires approximations, examined here.

3.3.2.2. Rate Constants for a Multistep Catalytic Reaction from CV. A multistep catalytic cycle generally cannot be described by a single step or rate constant but rather by a global rate constant k_{obs}(TOF_{max}, section 3.3.2.5), which can either be a composite of rate constants for the elementary steps within the cycle or reflect a rate-limiting step. In many cases, the E_rC_i' equations (eqs 10 and 12) presented above can be directly extended to multielectron, multistep reaction pathways; however, this is not universally true. Recently, Costentin and Savéant have reported the current–potential responses for several two-electron, two-step homogeneous molecular catalysis pathways to address this issue.[41] While we restrict our discussion here to these two-electron, two-step pathways (first presenting the heterolytic pathways and concluding with a brief discussion of homolytic reactions), a treatment similar to that presented in ref 41 can be extended to other multielectron, multistep reaction pathways.

The various possible reaction schemes considered here, including both heterolytic and homolytic pathways, are presented in Table 2. Each of these scenarios has both electron transfer steps and so-called chemical steps with corresponding rate constants. Of note, these chemical steps must not necessarily correspond to a single elementary step but can consist of any number of sequential elementary steps, the composite of which can be characterized by an apparent rate constant. As detailed below, derivatives of the E_rC_i' equations can be utilized to extract k_{obs} from the plateau current for

dx.doi.org/10.1021/ic500658x | Inorg. Chem. 2014, 53, 9983–10002

heterolytic reactions in limiting cases for which there is a rate-limiting chemical step. For intermediate cases, ref 41 provides the detailed expressions relating k_{obs} to the elementary rate constants k_1 and k_2. In some of these intermediate cases, k_{obs} cannot be immediately obtained from the plateau current. The homolytic case is treated separately, as described at the end of this section.

The heterolytic reaction pathways fall into two categories. In the first category, all electron transfers occur at the electrode, and in the second category, one electron transfer occurs in solution: 1 equiv of Q reduces a reaction intermediate (O, Q′, or Q″). The latter pathway is sometimes referred to as solution electron transfer (SET).[59] In cases where the second electron transfer is more difficult than the first, the homogeneous electron transfer pathway is unfavorable. In these cases, an irreversible one-electron *EC* wave precedes the catalytic wave; typically, k_1 can be determined from the positive shift of this peak upon the addition of a substrate.[41] In cases where electrode and homogeneous electron transfer pathways are both thermodynamically relevant, the preference for one pathway over another is typically controlled by the relative rates of the subsequent homogeneous reactions. For example, in an *ECEC* reaction, Q reacts with substrate A to form Q′ with rate constant k_1 and Q′ is further reduced to form intermediate B. When k_1 is fast, Q′ forms near the electrode and is reduced through a heterogeneous electron transfer process at the electrode. When k_1 is slow, Q diffuses away from the electrode before reacting with A, and the Q′ formed will react with a second 1 equiv of Q through a homogeneous electron transfer process with rate constant k_e. The relative rates of k_1 and k_e can be measured through various means[60] or voltammograms can be measured as a function of C_P^0 in order to distinguish these mechanisms.

Generally speaking, k_{obs} can be directly determined from the plateau for heterogeneous scenarios in which the rate of regeneration of P from Q is controlled by a rate-limiting chemical step (e.g., $k_2C_Z^0 \gg k_1C_A^0$ and $k_2C_Z^0 \ll k_1C_A^0$; see Table 2). Under these circumstances, the equations derived for E_rC_i' can be applied,[41] but the catalytic plateau current equations differ for systems in which all electron transfers occur at the electrode versus those in which homogeneous electron transfer processes dominate. For a general multielectron catalytic system, the number of unique electron-transfer processes that occur at the electrode per catalyst (n) and the catalyst equivalents used per turnover (n') are incorporated into eqs 10 and 12 (section 3.3.2.1), yielding eqs 13 and 14, respectively (an exception is highlighted in Table 2; accounting for this exception, this rule may be more generally stated to apply to any multielectron catalytic system in which the second electron transfer follows the rate-limiting step).[41,42,61] For example, in an *ECEC* reaction with one homogeneous electron transfer, only P is reduced at the electrode ($n = 1$) and 2 equiv of catalyst P are necessary for turnover ($n' = 2$). For an *ECEC* reaction with only electrode electron transfers, P and Q′ are both reduced at the electrode ($n = 2$), but only 1 equiv of catalyst P is necessary for turnover ($n' = 1$).

$$i_c = nFAC_P^0\sqrt{Dn'k_{obs}} \tag{13}$$

$$\frac{i_c}{i_p} = \frac{1}{0.446}\sqrt{\left(\frac{RT}{nF\upsilon}\right)n'k_{obs}} \tag{14}$$

In eq 10, it may be tempting to simply make $n = 2$ for both two-electron, two-step reaction schemes. However, recall from earlier discussions that k_{obs} represents the rate at which Q becomes P. In the example of an *ECEC* reaction with one homogeneous electron transfer, turnover is in a sense a bimolecular reaction for which the formation of 1 equiv of product requires 2 equiv of Q to be converted to P. Because this treatment of electrocatalytic systems has only recently been explicitly discussed in the literature,[41] Figure 4 is included to

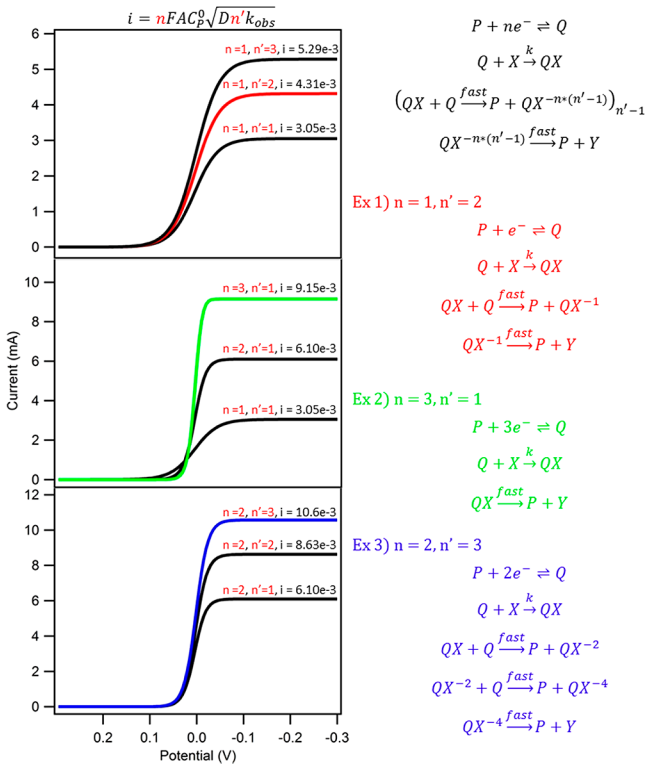

Figure 4. Simulations of the mechanism shown in the top right portion of the figure shown with the corresponding calculated current using eq 13 for the appropriate n and n'. Three example mechanisms are shown to further illustrate how the figures were simulated. $C_P^0 = 1 \times 10^{-6}$ mol cm^{-3}, $F = 96485$ C mol^{-1}, $A = 1$ cm^2, $C_X^0 = 1$ M, and $k = 100$ M^{-1} s^{-1}.

demonstrate the use of eq 13 on simulated data. In Figure 4, one mechanism has been presented in which the values of n and n' can be specified by simple alterations; the result of the simulations demonstrates the difference in CV responses and peak currents between the two scenarios. Namely, as the equation would suggest, the plateau current increases linearly with n and increases with $\sqrt{n'}$. If a mechanism is unknown and n is chosen as the number of total electron transfer processes, as has typically been done in the literature, k_{obs} will be underestimated by a factor of n if the process actually proceeds with homogeneous electron transfers. If the other extreme is taken, that is, n' is chosen as the number of total electron transfer processes, k_{obs} will be *overestimated* by a factor of n if the process actually proceeds with only electrode electron transfers. Wary experimenters unable to distinguish between electrode electron transfer and homogeneous electron transfer pathways may choose to set n equal to the total electron-transfer processes in order to avoid an overestimation of k_{obs}, but caution should be taken because no meaningful mechanistic

dx.doi.org/10.1021/ic500658x | Inorg. Chem. 2014, 53, 9983−10002

information can be gleaned from a rate constant determined with this estimate.

The discussion so far has highlighted that, for a two-electron, two-step heterolytic reaction, under the limiting scenarios in which there is a rate-limiting chemical step, k_{obs} can be determined from the plateau current and appropriate application of eqs 13 and 14. Under more complex scenarios, such as when the two chemical steps have comparable rate constants, k_{obs} can no longer be immediately obtained from the plateau current.[41] Under these circumstances, E_{cat}, $E_{cat/2}$, the plateau current, and information obtained from the foot-of-the-wave analysis (section 3.3.2.3) must all be used in conjunction to glean mechanistically relevant rate information. This topic is explored more fully in ref 41.

A homolytic reaction pathway has also been considered as a possible mechanism for H_2 evolution catalysis, specifically in the context of cobaloximes.[62−64] While digital simulations have been utilized to evaluate these pathways in CV responses, an equation describing the current−potential response has only recently been put forth.[41] Importantly, because of the second-order chemical step, the current response scales with the catalyst concentration to the 3/2 power (Table 2). This concentration dependence is also revealed to affect the overall shape of the catalytic sigmoid.[41]

3.3.2.3. Determining a Rate Constant for a Multistep Catalytic Reaction from CV: Competing Side Phenomena. Oftentimes, it is difficult to achieve the S-shaped catalytic response currents of zone KS. Competing side phenomena, such as substrate consumption, catalyst deactivation, and product inhibition, cannot always be eliminated through experimental parameters. Recently, however, a new method termed foot-of-the-wave analysis (FOWA) has been presented and applied by Savéant and Costentin to estimate kinetic information for electrochemical catalytic processes whose corresponding voltammograms do not meet the rigid requirements to be characterized as zone KS yet have an accessible "foot" to the catalytic wave (i.e., there are no redox events distorting the foot of the wave).[7,41,42,61] FOWA can be performed in two ways, depending on the reaction scenario. Here, FOWA is first derived for a case in which the first chemical step is rate determining. Subsequently, a standard FOWA which can be applied more generally is introduced.

FOWA begins with eq 15, which describes a catalytic response current for a multielectron, multistep reaction as a function of the potential obtained under the conditions of zone KS and the case in which the first chemical step is rate-determining (for the heterolytic reactions presented in Table 2, $k_2C_Z^0 \gg k_1C_A^0$) and $E_{cat/2} = E_{redox}$.

$$i = \frac{nFAC_P^0\sqrt{Dn'k_{obs}}}{1 + \exp\left[\frac{nF}{RT}(E - E_{redox})\right]} \quad (15)$$

When a catalytic plateau current is achieved under such conditions, the simpler eq 13 can be used to extract k_{obs} from i_c. However, perturbation of the response current by side phenomena, like substrate consumption and catalyst deactivation, becomes increasingly likely as the time course of the measurement proceeds, e.g., as the potential is scanned cathodically. FOWA analyzes the *idealized* catalyst reactivity by considering only the initial portion of the catalytic wave where it is expected that little to no substrate consumption, catalyst degradation, or other side phenomena have occurred.[42]

For normalization of eq 15 by i_p, the peak current in the absence of a substrate, as defined by eq 11, yields eq 16.

$$\frac{i}{i_p} = \frac{2.24\sqrt{\frac{RT}{nF\upsilon}}\sqrt{n'k_{obs}}}{1 + \exp\left[\frac{nF}{RT}(E - E_{redox})\right]} \quad (16)$$

Figure 5a presents data in the format of i/i_p versus $E - E_{redox}$. Under purely kinetic conditions with no substrate consumption, the classic sigmoidal current response is obtained, as predicted by eq 15; however, side phenomena cause the response current to deviate from the predicted S shape. In the example shown in Figure 5a, the influence of substrate consumption increases as the bulk substrate concentration decreases. FOWA assumes that catalysis is occurring under purely kinetic conditions at the foot of the wave, and this can be used to analyze voltammograms that deviate from the S-shaped wave of zone KS as a result of these undesired side phenomena.

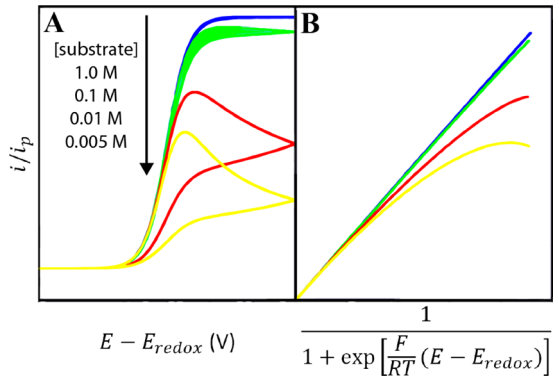

Figure 5. (A) Simulated CV responses for catalytic conversion of a substrate to a product with various concentrations of substrate (shown decreasing from blue to yellow), with $\upsilon = 0.1$ V s^{-1}, $D_P = 10^{-5}$ cm^2 s^{-1}, $C_P^0 = 1$ mM, $T = 298$ K, $n' = 2$, and $kC_A^0 = 50$ s^{-1}. (B) FOWA linear plots for the same CV responses showing the linear fits obtained. Adapted with permission from ref 42. Copyright 2012 American Chemical Society.

Replotting i/i_p versus $1/\{1 + \exp[(nF/RT)(E - E_{redox})]\}$ results in a straight line for response currents obtained under zone KS conditions (Figure 5b). Side phenomena result in deviation from the predicted linear relationship, but at the foot of the wave, the plot holds to the linear expectation. Thus, a linear extrapolation can be performed to retrieve the expected linear relationship had no side phenomena occurred. From eq 16 (eq 14 adjusted for potential dependence), we see that k_{obs} can be determined from the slope of this line $[m = 2.24(RT/nF\upsilon)^{1/2}(n'k_{obs})^{1/2}]$.[42] It is key to note that this method of FOWA can only be applied to the scenarios described above: the first chemical step is rate-limiting and $E_{cat/2} = E_{redox}$. The value for k_{obs} extracted from this analysis is, per Table 2, equal to $k_1C_A^0$ and describes the reactivity of the catalyst *in the hypothetical absence of side phenomena.*

FOWA expressions have also been presented for more general scenarios, which do not satisfy the conditions put forth above, including heterolytic pathways in which the second chemical step is rate-limiting, intermediate cases in which the first and second chemical steps have comparable rates, and the homolytic reaction pathway.[41] Unlike the derivation presented above, these expressions do not require that $E_{cat/2} = E_{redox}$, which is important because $E_{cat/2}$ cannot always be accurately or

dx.doi.org/10.1021/ic500658x | Inorg. Chem. 2014, 53, 9983−10002

Table 3. General Expressions for Foot-of-the-Wave Analysis ($E \gg E_{cat/2}$; Adapted from Reference 41)

Heterolytic Reaction Processes	
All electron transfers occur at the electrode	**One homogeneous electron transfer**
EECC	
$O + e \rightleftharpoons P \quad E^0_{O/P}$ $P + e \rightleftharpoons Q \quad E^0_{P/Q}$ $Q + A \longrightarrow B \quad k_1$ $B + Z \longrightarrow O + C \quad k_2$ $i \approx 2FAC_P^0\sqrt{D}\sqrt{k_1C_A^0}\exp\left[-\frac{F}{RT}(E - E^o_{P/Q})\right]$	$P + e \rightleftharpoons Q \quad E^0_{P/Q}$ $Q + A \longrightarrow B \quad k_1$ $B + Z \longrightarrow O + C \quad k_2$ $O + Q \longrightarrow 2P$ See Ref. 41
ECEC, $E^o_{P/Q} < E^o_{Q'/B}$	
$P + e \rightleftharpoons Q \quad E^0_{P/Q}$ $Q + A \longrightarrow Q' \quad k_1$ $Q' + e \rightleftharpoons B \quad E^0_{Q'/B}$ $B + Z \longrightarrow P + C \quad k_2$ $i \approx 2FAC_P^0\sqrt{D}\sqrt{k_1C_A^0}\exp\left[-\frac{F}{RT}(E - E^o_{P/Q})\right]$	$P + e \rightleftharpoons Q \quad E^0_{P/Q}$ $Q + A \longrightarrow Q' \quad k_1$ $Q' + Q \longrightarrow P + B \quad k_e$ $B + Z \longrightarrow P + C \quad k_2$ $i \approx FAC_P^0\sqrt{D}\sqrt{2k_1C_A^0}\exp\left[-\frac{F}{RT}(E - E^o_{P/Q})\right]$
ECCE, $E^o_{P/Q} < E^o_{Q''/P}$	
$P + e \rightleftharpoons Q \quad E^0_{P/Q}$ $Q + A \longrightarrow B \quad k_1$ $B + Z \longrightarrow Q'' \quad k_2$ $Q'' + e \rightleftharpoons P + C \quad E^0_{P/Q''}$ $i \approx 2FAC_P^0\sqrt{D}\sqrt{k_1C_A^0}\exp\left[-\frac{F}{RT}(E - E^o_{P/Q})\right]$	$P + e \rightleftharpoons Q \quad E^0_{P/Q}$ $Q + A \longrightarrow B \quad k_1$ $B + Z \longrightarrow Q'' \quad k_2$ $Q'' + Q \longrightarrow 2P + C \quad k_e$ $i \approx FAC_P^0\sqrt{D}\sqrt{2k_1C_A^0}\exp\left[-\frac{F}{RT}(E - E^o_{P/Q})\right]$
ECCE, $E^o_{P/Q} > E^o_{Q''/P}$ *electron transfer at electrode only, unfavorable homogeneous electron transfer pathway*	
$P + e \rightleftharpoons Q \quad E^0_{P/Q}$ $Q + A \longrightarrow B \quad k_1$ $B + Z \longrightarrow Q'' \quad k_2$ $Q'' + e \rightleftharpoons P + C \quad E^0_{Q''/P+C}$	$\ln(i) = \ln\left(2FAk_SC_P^0\sqrt{D}\right) - \frac{\alpha F}{RT}\left(E - E^o_{Q''/P+C}\right)$
ECEC, $E^o_{P/Q} > E^o_{Q'/B}$ *electron transfer at electrode only, unfavorable homogeneous electron transfer pathway*	
$P + e \rightleftharpoons Q \quad E^0_{P/Q}$ $Q + A \longrightarrow Q' \quad k_1$ $Q' + e \rightleftharpoons B \quad E^0_{Q'/B}$ $B + Z \longrightarrow P + C \quad k_2$	$i \approx 2FAC_P^0\sqrt{D}\sqrt{k_2C_Z^0}\exp\left[-\frac{F}{RT}\left(E - E^o_{Q'/B}\right)\right]$
Homolytic Reaction Process	
$P + e \rightleftharpoons Q \quad E^0_{P/Q}$ $Q + A \underset{k_{-1}}{\overset{k_1}{\rightleftharpoons}} B$ $B + B \xrightarrow{k_d} 2P + C$	$i \approx FA\sqrt{\frac{4Dk_d}{3}}\frac{k_1C_A^0}{k_{-1}}(C_P^0)^{\frac{3}{2}}\exp\left[-\frac{3F}{2RT}(E - E^o_{P/Q})\right]$

directly determined from CV if side phenomena are active. While detailed derivations of these FOWA expressions are beyond the scope of this viewpoint and presented elsewhere,[41] their derivation can be summarized as follows. The current–potential responses for most of the scenarios in Table 2 take the form of eq 17, where the expressions for i_c and $E_{cat/2}$ are unique to each specific scenario.

$$i = \frac{i_c}{1 + \exp\left[\frac{F}{RT}(E - E_{cat/2})\right]} \tag{17}$$

At the foot of the wave, $E \gg E_{cat/2}$, and thus $\exp[F/RT(E - E_{cat/2})] \gg 1$. This approximation provides the current–potential approximation presented in eq 18.

dx.doi.org/10.1021/ic500658x | Inorg. Chem. 2014, 53, 9983−10002

$$i \approx i_c \exp\left[-\frac{F}{RT}(E - E_{cat/2})\right] \quad (18)$$

Substitution of the expressions for i_c and $E_{cat/2}$ provides the general expressions for the foot-of-the-wave analysis presented in Table 3. With the current versus $\exp[(F/RT)(E - E_{cat/2})]$ plot, rate information can be gleaned from the slope of the resulting linear region at the foot of the wave. It is key to note that application of FOWA can generally only provide rate information for the chemical step immediately following E_{redox}. This is demonstrated for the *EECC* case, with all electron transfers occurring at the electrode in Figure 6.

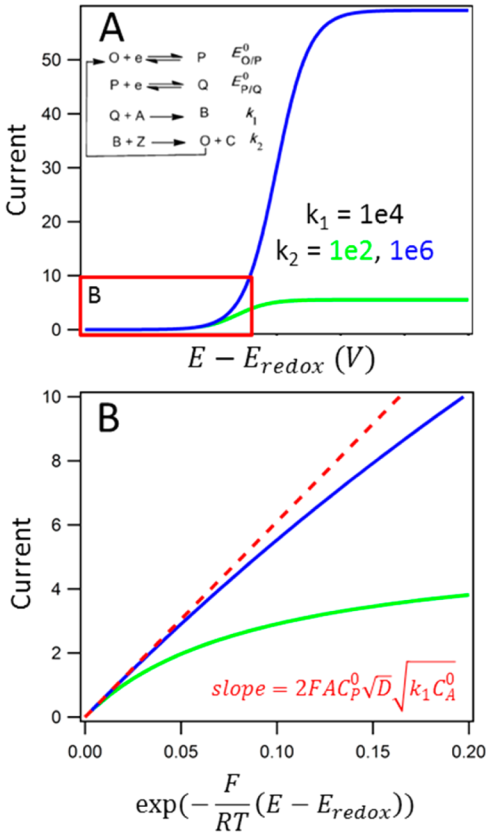

Figure 6. (A) CV response for the *EECC* case with no substrate depletion in the cases that k_2 (green) and k_1 (blue) are rate-limiting. (B) FOWA revealing that the linear region corresponds to k_1 regardless of the rate-determining step.

3.3.2.4. Evaluating Kinetics via Digital Simulations. Electrochemical simulation software (e.g., *DigiElch* and *DigiSim*) allows the input of initial conditions like concentrations, standard potentials, and cell parameters, as well as the proposed mechanism by which a reaction is thought to proceed. Rate constants must accompany each step, but most simulation software programs are able to perform a "best fit" in order to determine rate constants. It is important to remember that a direct match of voltammograms does not guarantee a direct match of the mechanism, just as is true for any other form of mechanistic analysis. In order to appropriately use electrochemical simulation software, rigorous analysis of the catalyst and its reactivity is essential in order to establish a mechanistic proposal. All rate constants for individual steps within the proposed mechanism which can be determined experimentally should be, in order to enhance the accuracy of other rate constants determined via simulation. This may include performing familiar methods of mechanistic analysis, such as equilibrium and rate constant determination through NMR studies,[65] stoichiometric electrolysis, stopped-flow measurements, or laser flash-quench studies[60] coupled with transient absorption spectroscopy. Additionally, voltammograms should be collected at multiple scan rates, catalyst concentrations, and substrate concentrations and fit globally across these parameters.

CV is extremely sensitive to reaction environments; consequently, the shape of the wave can be influenced by minor phenomena. Modeling each step of the core mechanism, therefore, is typically not enough to properly model the experimental voltammogram. Side processes, such as substrate consumption, homo- and heteroconjugation of the acid, or any alternative pathway that may affect the current (e.g., catalyst degradation processes, formation of spectator species, etc.) must be factored into the simulation; several programs permit simulation of these side phenomena.[66,67] We refer the reader to the elegant examples of kinetic analysis via digital simulation of CV available in refs 66−68 for additional details.

3.3.2.5. Determining TOF from k_{obs}. In molecular electrocatalysis, TOF is a kinetic parameter that reflects the catalytic activity and is parametrized by the applied potential. In its most general definition, TOF is the number of moles of product produced per unit time per mole of catalyst *contained in the reaction−diffusion layer* (not the bulk solution). As noted by Savéant and Costentin, obtaining TOF from only the reactions occurring at the electrode surface provides a complete picture of the catalyst properties.[7] In many reports, TOF has been simply equated directly to the observed rate constant (k_{obs}), which can often be obtained from the plateau current of cyclic voltammograms measured under the conditions set forth in sections 3.3.2.1−3, namely pure kinetic conditions and no substrate consumption. This is a limiting value wherein TOF is constrained by the potential-independent rate constant for chemical regeneration of P (k_{obs}) and is better defined as TOF_{max}.[41]

In the region of CV where the catalytic current has not yet reached its plateau, TOF is dependent on the applied potential E and reflects the percentage of activated catalyst (Q). In cases where all electron transfers are Nernstian, the relationship is described by eq 19.[7,41,42] When the applied potential is significantly negative of $E_{cat/2}$ (the half-wave potential of the steady-state catalytic wave and the point at which 50% of the catalyst is activated), eq 19 shows that TOF becomes independent of the overpotential and reaches a TOF_{max} value. For all cases presented in Tables 2 and 3, except an *EECC* reaction with homogeneous electron transfer and a homolytic process, TOF_{max} is defined by eq 20. When $k_1C_A^0$ or $k_2C_Z^0$ is rate-limiting, TOF_{max} can be simplified to the k_{obs} expressions shown in Table 2.

$$TOF = \frac{TOF_{max}}{1 + \exp\left[\frac{F}{RT}(E - E_{cat/2})\right]} \quad (19)$$

$$TOF_{max} = \frac{k_1 k_2 C_A^0 C_Z^0}{k_1 C_A^0 + k_2 C_Z^0} \quad (20)$$

Equation 19 can be reformulated by incorporating the parameter η (section 3.3.1.1) to provide a valuable TOF−η relationship (eq 21).[41,42]

dx.doi.org/10.1021/ic500658x | Inorg. Chem. 2014, 53, 9983−10002

$$\mathrm{TOF} = \frac{\mathrm{TOF_{max}}}{1 + \exp\left[\frac{F}{RT}(E - E_{\mathrm{cat}/2})\right]} = \frac{\mathrm{TOF_{max}}}{1 + \exp\left[\frac{F}{RT}(E^{\circ}_{\mathrm{A/B}} - E_{\mathrm{cat}/2})\right]\exp\left(-\frac{F}{RT}\eta\right)} \quad (21)$$

An *ECCE* mechanism wherein the second electron transfer is more difficult than the first is one exception to the general application of eqs 19 and 21, and the TOF–η relationship for this scenario is described by eq 22, where α is a transfer coefficient, which reflects the fact that the second electron transfer is a dissociative electron transfer reaction and does not obey the Nernst law.[41]

$$\mathrm{TOF} = \frac{\mathrm{TOF_{max}}}{1 + \exp\left[\alpha\frac{F}{RT}(E - E_{\mathrm{cat}/2})\right]} \quad (22)$$

For the other exception defined in the literature—a homolytic process—the TOF–η relationship is described by eq 23 and accounts for the second-order (in catalyst) chemical step.

$$\mathrm{TOF} = \frac{\mathrm{TOF_{max}}}{\left\{1 + \exp\left[\frac{F}{RT}(E - E_{\mathrm{cat}/2})\right]\right\}^{3/2}} \quad (23)$$

The TOF–η relationship (eq 21) introduced by Costentin and Savéant provides a means for comparing catalysts at various overpotentials. Equation 21, which includes the standard potential for substrate conversion $E^{\circ}_{\mathrm{A/B}}$, underscores that once the applied overpotential is equal to $E_{1/2}$, TOF equals $^1/_2$ $\mathrm{TOF_{max}}$ (for a homolytic process, $0.35\mathrm{TOF_{max}}$).[41,42] As noted above, the potential-dependent region reflects the percentage of active catalyst. For the general cases, the slope of this region is equal to $F/(RT \ln 10)$. For an *ECCE* reaction scheme in which the second electron transfer is more difficult than the first, the slope is $\alpha[F/(RT \ln 10)]$, while for a homolytic reaction, the slope is $3F/(2RT \ln 10)$.

Figure 7 illustrates the result of applying eq 21 to two catalysts with different $E^{\circ}_{\mathrm{P/Q}}$ and $k_{\mathrm{obs}}(\mathrm{TOF_{max}})$ values reducing the same substrate. These TOF–η plots can provide for a means of assessing at which potentials—for a specific catalytic transformation—different catalysts will be most useful. For example, η for electrolysis can be optimized or a desired TOF can be identified.

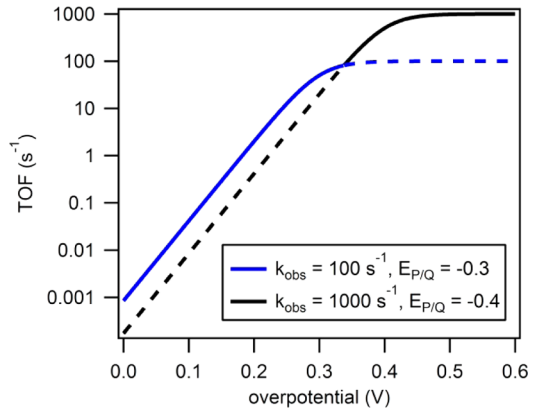

Figure 7. Plots of TOF versus applied overpotential for two catalysts with different values of k_{obs} and $E^{\circ}_{\mathrm{P/Q}}$, demonstrating the relationship between TOF and applied overpotential. The zero overpotential intercept yields $\mathrm{TOF_0}$, and at the plateau, TOF is equal to k_{obs}. The solid region lines indicate which catalyst has a higher TOF at a specific overpotential, showing that while the catalyst shown in blue has a larger $\mathrm{TOF_0}$, the catalyst shown in black has a higher $\mathrm{TOF_{max}}$.

The metric $\mathrm{TOF_0}$ has also been proposed: the extrapolated TOF at $E = E^{\circ}_{\mathrm{A/B}}$.[41,42] For the general cases, this relationship is described by eq 24.

$$\mathrm{TOF_0} = \mathrm{TOF_{max}}\exp\left[-\frac{F}{RT}(E^{\circ}_{\mathrm{A/B}} - E_{\mathrm{cat}/2})\right] \quad (24)$$

While $\mathrm{TOF_0}$ has been described as a method to determine which catalysts are inherently "good" and inherently "bad",[42] it has been noted that, because $\mathrm{TOF_0}$ depends on the location of zero overpotential, utilizing different substrates with different values of $E^{\circ}_{\mathrm{A/B}}$ may flip which catalyst is the "better" catalyst.[69] Also, as noted earlier, the slope of the TOF–η relationship can be mechanism-dependent, which will severely skew the perception gleaned from $\mathrm{TOF_0}$. $\mathrm{TOF_0}$ does not capture the possibility that substrates with different values of $E^{\circ}_{\mathrm{A/B}}$ can accelerate or decelerate the homogeneous rate-determining step, altering the rate of catalysis. Additionally, as noted in the introduction of $\mathrm{TOF_0}$,[42] the value of $\mathrm{TOF_0}$ is dependent on the substrate concentration, and $\mathrm{TOF_0}$ values spanning 3 orders of magnitude were found in the system studied where the substrate concentration was varied over 2 orders of magnitude. This inherent dependence of $\mathrm{TOF_0}$ on both the substrate identity and concentration underscores the need to compare catalysts with the same catalyst concentration, substrate, and substrate concentration. It is unlikely that literature catalysts will have been studied with identical substrate identity and concentration, meaning this metric is only useful for benchmarking in highly specific instances such as in dedicated catalyst comparison studies.

While kinetic parameters (k_{obs}, $\mathrm{TOF_{max}}$, and TOF–η relationships) are valuable figures of merit, it is our view that their absolute magnitude is not the most meaningful metric for comparison because it is often situation-dependent (e.g., substrate concentration). More consequential is the mechanistic information that can be gleaned from analysis of the reaction kinetics. This information can yield a rate law or rate constants, parameters that provide more meaningful insight into the catalyst performance.

3.4. Case Studies. Application of the methods of analysis presented in section 3.3 to molecular electrocatalysts for H_2 generation and other multielectron, multistep reaction schemes can provide important kinetic and mechanistic information. Challenges to this process include recognizing, minimizing, and accounting for competing side phenomena in the analysis. In this section, we first present a series of simulated voltammograms that clearly illustrate the influence of deleterious side phenomena on catalysis. Then we provide a case study that illustrates how competing side phenomena can be accounted for, how a global catalytic rate constant can be derived for a complex multielectron, multistep reaction scheme, and how valuable mechanistic information can be garnered from a readily obtained set of cyclic voltammograms.

3.4.1. Illustrative Examples of Nonidealized Cyclic Voltammograms. The catalytic S-shaped voltammograms in zone KS of Figure 3 are described by eq 10, where the plateau catalytic current is dependent on the surface area of the electrode, the diffusion coefficient of the catalyst, the number of electrons involved, and the observed rate. While this predicted catalytic response current is conceptually easy to interpret, very

dx.doi.org/10.1021/ic500658x | Inorg. Chem. 2014, 53, 9983−10002

seldom does an experiment actually give a CV response that is a perfect "S". Substrate depletion within the reaction layer can cause the pseudo-first-order assumptions of eq 10 to break down, and various side phenomena, such as catalyst decomposition or product inhibition, can occur, preventing the S-shaped voltammogram from being achieved. As examined below, analysis of these perturbed catalytic currents directly with eq 10 leads to inaccurate figures of merit and incorrectly interpreted mechanisms.

Per eq 10, the catalytic current i_c should not depend on the scan rate. Figure 8 shows simulated cyclic voltammograms for an E_rC_i' mechanism at various scan rates. At 100 V s^{-1}, the response is the predicted S-shape voltammogram, with the reverse trace nearly overlaying the forward scan. When the scan rate is slowed, three differences are apparent: the voltammogram has a peak shape indicative of zone K, the current maximum decreases with decreasing scan rate, and the reverse scan does not overlap with the forward scan. When the peak current versus scan rate is plotted, as shown for the simulated voltammograms (Figure 8, inset) and the $[Ni(7P^{Ph}{}_2N^{C_6H_4Br})_2]^{2+}$ catalyst (Figure 9), both scan-rate-dependent and scan rate-independent regions are observed. At slower scan rates, the measurement takes more time and the substrate is depleted within the reaction layer, preventing the pseudo-first-order conditions necessary for eq 10 from being met. By contrast, at faster scan rates, the overall measurement time is shorter, the substrate is not substantially depleted over the course of the experiment, and pseudo-first-order conditions hold. In order to correctly determine the observed rate constant from a cyclic voltammogram, the catalytic response current must be scan rate-independent. Cyclic voltammograms for catalytic systems should always be analyzed at various scan rates in order to determine the scan rate-independent region and an appropriate scan rate at which to carry out analysis.

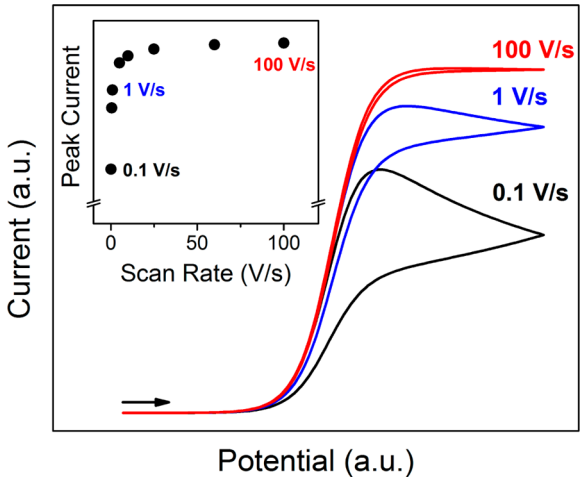

Figure 8. Cyclic voltammograms for an E_rC_i' mechanism showing a transition from zone K to zone KS with increasing scan rates. At even higher scan rates (not shown), zone KD is reached. Inset graph: peak current as a function of the scan rate. Simulated with *DigiElch*: $\alpha = 0.5$, k_s = 10,000 cm s^{-1}, k_e = 100,000 M^{-1} s^{-1}, [catalyst] = 0.002 M, and $[substrate]_0$ = 1 M.

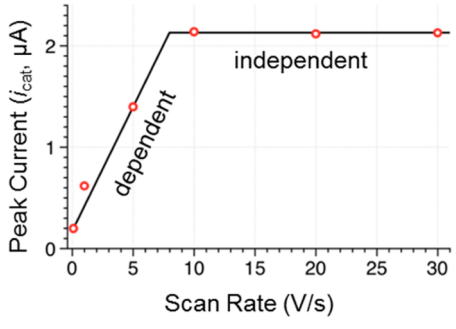

Figure 9. Scan rate dependence of the peak catalytic current i_{cat} for a nickel H_2 evolution electrocatalyst with acid in acetonitrile. Both scan rate-dependent and -independent regions are observed. Adapted with permission from ref 47. Copyright 2013 American Chemical Society.

In addition to causing inaccurate estimates of the catalytic rate, substrate depletion can also lead to incorrect determination of the reaction order in the substrate and catalyst. Figure 10 shows simulated cyclic voltammograms for an E_rC_i' mechanism at three different catalyst concentrations, with (Figure 10c) and without (Figure 10a) substrate depletion. When substrate depletion is not present, the voltammetric response is an S-shaped wave and the peak current has first-order dependence on the catalyst concentration (Figure 10b). However, when substrate is depleted during the experiment, the voltammetric response is a classic deviation from an S-shaped wave: the current does not plateau nor does the return trace follow the forward trace. Further, analysis of the peak current results in an apparent dependence on the catalyst concentration that is less than first order. Measurement of the current response as a function of the scan rate should reveal whether or not substrate consumption is perturbing the voltammograms.

Catalyst decomposition can also induce significant deviations from S-shaped voltammograms during the time course of typical CV. Figure 11 shows CV responses for an E_rC_i' mechanism where the reduced catalyst Q can decompose by rate constant k_{decomp}. In the example shown, with a fast catalytic rate constant (k_e = 100,000 M^{-1} s^{-1}), values of k_{decomp} as low as 30 s^{-1} result in non-S-shaped cyclic voltammograms. The impact of catalyst decomposition may be diminished at faster scan rates.

3.4.2. Mechanistic and Kinetic Insights into a CO_2 Reduction Catalyst. A recent example by Costentin et al. demonstrates the translation of the concepts presented in section 3.3 from their theoretical origins to application in mechanistic analysis.[61] The system of interest is the two-electron reduction of CO_2 to CO with an iron tetraphenylporphyrin (FeTPP) catalyst and a Bronsted acid cocatalyst. This work highlights both the experimental niceties required for obtaining the observed rate constant and subsequent elucidation of relevant mechanistic information. The first point of interest in this example is the lack of an S-shaped catalytic response in CV. As noted above, this is a common occurrence in electrocatalysis and, for reasons that have already been discussed, precludes the use of the plateau equations. The authors turned to the FOWA method, outlined in section 3.3.2.3, and utilized this method to obtain the observed rate of catalysis.

The data presented for this case cannot be considered the "ideal" scenario (Figure 12; catalysis occurs at the Fe^I/Fe^0 couple rather than the Fe^{II}/Fe^I couple) for use of the FOWA method, so it is important to first demonstrate that the authors are able to apply it accurately through practical considerations. The active form of the catalyst is Fe^0TPP; however, as prepared, the catalyst is in the Fe^{II} oxidation state. $Fe^{II}TPP$

dx.doi.org/10.1021/ic500658x | Inorg. Chem. 2014, 53, 9983−10002

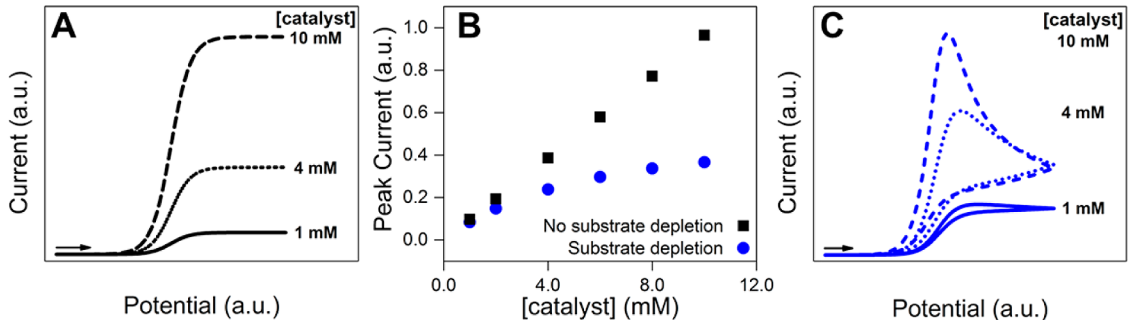

Figure 10. Cyclic voltammograms as a function of the catalyst concentration for an E_rC_i' mechanism with (A) no substrate depletion and (C) substrate depletion. The middle graph (B) shows the peak current as a function of the catalyst concentration for scenarios a and c, demonstrating that less than first order in catalyst may be observed when substrate is depleted over the course of the voltammogram. Simulated with *DigiElch*: α = 0.5, k_s = 10,000 cm s^{-1}, scan rate = 0.2 V s^{-1}, k_e = 100,000 M^{-1} s^{-1}, and $[substrate]_0$ = 1 M. In scenario a, the concentration of the substrate was not permitted to vary over the course of the scan.

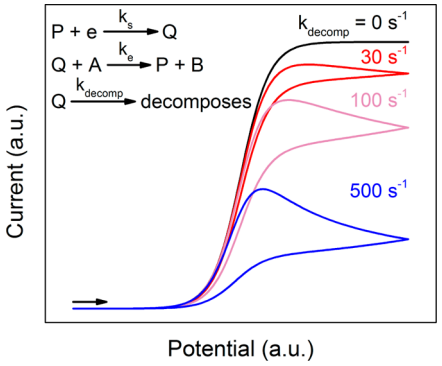

Figure 11. Simulated cyclic voltammograms for an E_rC_i' mechanism as a function of the decomposition rate for the reduced catalyst Q. Simulated with *DigiElch*: α = 0.5, k_s = 10,000 cm s^{-1}, scan rate = 0.2 V s^{-1}, k_e = 100,000 M^{-1} s^{-1}, $[catalyst]_0$ = 0.002 M, and $[substrate]_0$ = 1 M. The concentration of the substrate was not permitted to vary over the course of the scan.

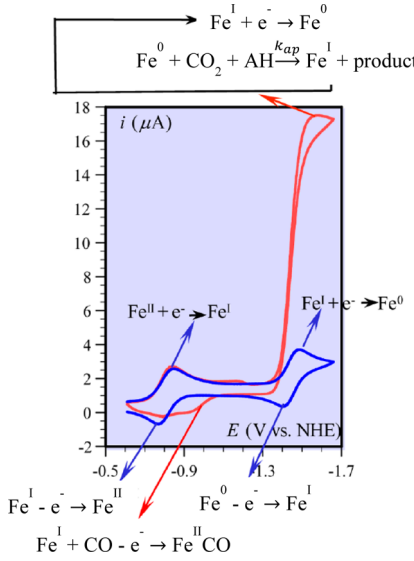

Figure 12. Select voltammograms showing the reversible Fe^{II}/Fe^{I} and Fe^{I}/Fe^{0} waves (blue) and the catalytic wave after the addition of CO_2 and a proton source (red). Adapted with permission from ref 61. Copyright 2013 American Chemical Society.

undergoes two reversible single-electron transfers to reach the active state, which presents two problems for FOWA. First, the noncatalytic redox activity will interfere with the linear regression. The authors circumvent this by splicing the data, removing the region related to the Fe^{II}/Fe^{I} couple, so that analysis is only performed on data surrounding the Fe^{I}/Fe^{0} couple. This still leaves the residual current from diffusion of Fe^{II}, but this has a negligible effect on the overall analysis. The second problem is that i_p, as defined for FOWA, is used to cancel the concentration and diffusion coefficient of the catalyst; this relies on the assumption that the peak current is generated from a single-electron Nernstian wave with no other influences. In this example, the Fe^{I}/Fe^{0} couple is a single-electron Nernstian wave but overlaps the Fe^{II}/Fe^{I} diffusional tail as noted above. Although the diffusional tail has a negligible effect with respect to the catalytic current, it is not negligible in the absence of substrate. The authors resolve this by using the peak current from the Fe^{II}/Fe^{I} wave for i_p. With these considerations, FOWA was performed.

The results of FOWA were interpreted using a global catalytic rate constant (k_{obs}), derived from the proposed mechanism (Scheme 1) through the application of steady-state approximations to the reaction intermediates. Here, the

Scheme 1[a]

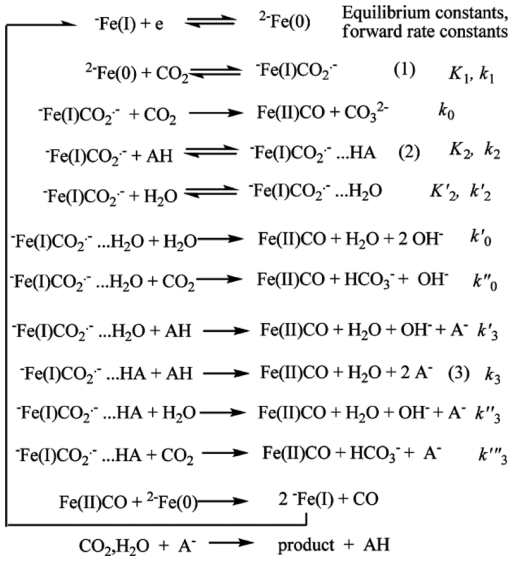

[a]Reprinted with Permission from Reference 61. Copyright 2013 American Chemical Society.

dx.doi.org/10.1021/ic500658x | Inorg. Chem. 2014, 53, 9983−10002

concentrations of substrate (CO_2) and cocatalysts (HA and H_2O) were considered constant within the reaction diffusion layer (and equal to bulk concentrations). Importantly, k_{obs} was derived from Fick's laws of diffusion, and as a result, the rate equation required that the catalyst and substrate concentration parameters be separated (i.e., k_{obs} must not contain the catalyst concentration as a parameter). This was achieved by careful substitution of variables and select approximations to yield k_{obs}. By variation of the concentrations of substrate (CO_2) and cocatalysts (HA and H_2O), the specific roles of the cocatalysts were probed, detailed mechanistic information was revealed, and a rate-determining, concerted proton−electron transfer bond cleavage reaction was identified.

In summary, this example is a clear illustration of how a global catalytic rate constant can be derived for a complex reaction and valuable kinetic and mechanistic data can be extracted from nonidealized (S-shaped) CV responses.

$$k_{obs} = K_1\left\{k_0[CO_2] + \frac{k_2'[H_2O]_r(k_0'[H_2O]_r + k_0''[CO_2]_r)}{k_{-2}' + k_3'[AH]} + \left[\frac{k_2(k_3''[H_2O]_r + k_3'''[CO_2])}{k_{-2} + k_3[AH]} + \frac{k_2'[H_2O]_r k_3'}{k_{-2}' + k_3'[AH]}\right][AH] + \frac{k_2k_3}{k_{-2} + k_3[AH]}[AH]^2\right\}$$

4. CONCLUSION

It is hoped that careful electrochemical studies of new molecular electrocatalysts will help realize large-scale clean-fuel production and assist in the understanding of enzyme mechanisms. Electrochemical techniques, in particular CV as discussed here, are powerful characterization tools. Tempering this claim is the realization that no single method for accurately determining electrochemical catalytic rate constants exists because many molecular electrocatalysts proceed through complex multistep pathways possibly involving side reactions, resulting in complex CV responses. Kinetic parameters can be determined or estimated by the methods reviewed here. Experimenters should be certain that analyses of voltammograms are performed on data obtained under appropriate conditions. Further, it is imperative that reports of catalysis are accompanied by details of reaction conditions and analysis methods employed in order to more readily compare catalysts.

AUTHOR INFORMATION

Corresponding Author

*E-mail: dempseyj@email.unc.edu.

Notes

The authors declare no competing financial interest.

Biographies

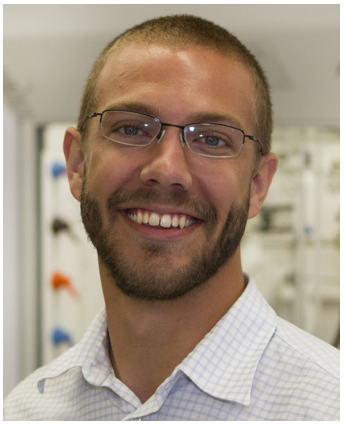

Eric S. Rountree was born in Elizabeth City, NC, in 1990. He received his bachelor's degree in chemistry, summa cum laude, in the spring of 2012 from North Carolina State University under the advisement of Prof. James D. Martin. Eric began his research in the Dempsey Lab in the summer of 2012, for which he received the Duke Energy Progress Graduate Fellowship in the summer of 2013 and the Richard G. Hiskey Research Fellowship in the summer of 2014.

Born in 1989 in Hillsboro, OR, Brian McCarthy began studying chemistry in the group of Prof. Carl Wamser at Portland State University. At the Massachusetts Institute of Technology, he worked first in the group of Prof. Daniel Nocera and later with Prof. Mircea Dincă, earning a chemistry S.B. in 2012. Brian is currently studying electrochemical processes as an DOE Office of Science Graduate Fellow in the group of Prof. Jillian Dempsey.

Thomas T. Eisenhart was born in Norman, OK, in 1988. He completed his B.S. in Chemistry, summa cum laude, in 2010 under the direction of Dr. Shannon Davis at Georgia Southern University. He

received a Rotary Ambassadorial Scholarship to study at Queen's University Belfast where he received his M.Sc. in 2010 under the tutelage of Dr. Andrew Marr. He began his Ph.D. with Prof. Jillian Dempsey at the University of North Carolina at Chapel Hill in 2011.

Jillian L. Dempsey was born in Summit, NJ, in 1982. She received her S.B. from the Massachusetts Institute of Technology in 2005 where she worked in the laboratory of Prof. Daniel G. Nocera. As an NSF Graduate Research Fellow, she carried out research with Prof. Harry B. Gray and Dr. Jay R. Winkler at the California Institute of Technology. In 2011 she received her Ph.D. and was awarded the Herbert Newby McCoy Award for Outstanding Achievements in Chemistry. From 2011 to 2012 she was an NSF ACC Postdoctoral Fellow with Prof. Daniel R. Gamelin at the University of Washington. In 2012 she joined the faculty at the University of North Carolina at Chapel Hill. Her research group explores charge transfer processes relevant to solar energy capture and conversion.

■ ACKNOWLEDGMENTS

We acknowledge the University of North Carolina for support of this work. E.S.R. gratefully acknowledges support from a Duke Energy Progress Environmental fellowship. B.D.M. gratefully acknowledges support from the Department of Energy Office of Science Graduate Fellowship Program (DOE SCGF), made possible in part by the American Recovery and Reinvestment Act of 2009, administered by ORISE-ORAU under Contract DE-AC05-06OR23100. We thank Prof. James M. Mayer, Dr. Charles C. L. McCrory, Prof. Royce W. Murray, Prof. Yogesh Surendranath, Prof. Jenny Y. Yang, and Prof. Aaron K. Vanucci for insightful discussions.

■ REFERENCES

(1) Vignais, P. M.; Billoud, B. *Chem. Rev.* **2007**, *107*, 4206−4272.
(2) Wang, M.; Chen, L.; Sun, L. *Energy Environ. Sci.* **2012**, *5*, 6763−6778.
(3) Thoi, V. S.; Sun, Y.; Long, J. R.; Chang, C. J. *Chem. Soc. Rev.* **2013**, *42*, 2388−2400.
(4) Felton, G. A. N.; Mebi, C. A.; Petro, B. J.; Vannucci, A. K.; Evans, D. H.; Glass, R. S.; Lichtenberger, D. L. *J. Organomet. Chem.* **2009**, *694*, 2681−2699.
(5) Dempsey, J. L.; Winkler, J. R.; Gray, H. B. In *Comprehensive Inorganic Chemistry II*; Reedijk, J., Poeppelmeier, K., Eds.; Elsevier: Oxford, U.K., 2013; Vol. *8*, pp 553−565.
(6) Benson, E. E.; Kubiak, C. P.; Sathrum, A. J.; Smieja, J. M. *Chem. Soc. Rev.* **2009**, *38*, 89−99.
(7) Costentin, C.; Robert, M.; Savéant, J.-M. *Chem. Soc. Rev.* **2013**, *42*, 2423−2436.
(8) Wasylenko, D. J.; Palmer, R. D.; Berlinguette, C. P. *Chem. Commun.* **2013**, *49*, 218−227.
(9) Concepcion, J. J.; Jurss, J. W.; Brennaman, M. K.; Hoertz, P. G.; Patrocinio, A. O. T.; Murakami Iha, N. Y.; Templeton, J. L.; Meyer, T. J. *Acc. Chem. Res.* **2009**, *42*, 1954−1965.
(10) Pinaud, B. A.; Benck, J. D.; Seitz, L. C.; Forman, A. J.; Chen, Z.; Deutsch, T. G.; James, B. D.; Baum, K. N.; Baum, G. N.; Ardo, S.; Wang, H.; Miller, E.; Jaramillo, T. F. *Energy Environ. Sci.* **2013**, *6*, 1983−2002.
(11) Sathrum, A. J.; Kubiak, C. P. *J. Phys. Chem. Lett.* **2011**, 2372−2379.
(12) Lewis, N. S.; Nocera, D. G. *Proc. Natl. Acad. Sci. U. S. A.* **2006**, *103*, 15729−15735.
(13) Gray, H. B. *Nat. Chem.* **2009**, *1*, 7.
(14) Evans, D. H.; O'Connell, K. M.; Petersen, R. A.; Kelly, M. J. *J. Chem. Educ.* **1983**, *60*, 290−293.
(15) Mabbott, G. A. *J. Chem. Educ.* **1983**, *60*, 697−702.
(16) Compton, R. G.; Banks, C. E. *Understanding Voltammetry*, 2nd ed.; Imperial College Press: London, 2011.
(17) Kissinger, P. T.; Heineman, W. R. *J. Chem. Educ.* **1983**, *60*, 702−706.
(18) Izutsu, K. *Electrochemistry in Nonaqueous Solutions*; Wiley-VCH Verlag GmbH & Co. KGaA: Weinheim, Germany, 2003.
(19) Sawyer, D. T.; Sobkowiak, A.; Roberts, J. L. *Electrochemistry for Chemists*, 2nd ed.; John Wiley & Sons, Inc.: New York, 1995.
(20) Bard, A. J.; Faulkner, L. R. *Electrochemical Methods: Fundamentals and Applications*, 2nd ed.; John Wiley & Sons, Inc.: Hoboken, NJ, 2001.
(21) Myland, J. C.; Oldham, K. B. *Anal. Chem.* **2000**, *72*, 3972−3980.
(22) McCarthy, B. D.; Martin, D. J.; Rountree, E. S.; Ullman, A. C.; Dempsey, J. L. *Inorg. Chem.* **2014**, *53*, 8350−8361.
(23) Ramette, R. W. *J. Chem. Educ.* **1987**, *64*, 885.
(24) Pavlishchuk, V. V.; Addison, A. W. *Inorg. Chim. Acta* **2000**, *298*, 97−102.
(25) Gritzner, G.; Kuta, J. *Pure Appl. Chem.* **1984**, *56*, 461−466.
(26) Gagne, R. R.; Koval, C. A.; Lisensky, G. C. *Inorg. Chem.* **1980**, *19*, 2854−2855.
(27) Connelly, N. G.; Geiger, W. E. *Chem. Rev.* **1996**, *96*, 877−910.
(28) Felton, G. A. N.; Glass, R. S.; Lichtenberger, D. L.; Evans, D. H. *Inorg. Chem.* **2006**, *45*, 9181−9184.
(29) Roberts, J. A. S.; Bullock, R. M. *Inorg. Chem.* **2013**, *52*, 3823−3835.
(30) Fourmond, V.; Jacques, P.-A.; Fontecave, M.; Artero, V. *Inorg. Chem.* **2010**, *49*, 10338−10347.
(31) Kaupmees, K.; Kaljurand, I.; Leito, I. *J. Phys. Chem. A* **2010**, *114*, 11788−11793.
(32) Coetzee, J. F. In *Progress in Physical Organic Chemistry*; Streitwieser, A., Jr.; Taft, R. W., Eds.; John Wiley & Sons, Inc.: Hoboken, NJ, 1967; Vol. *4*, pp 45−92.
(33) Helm, M. L.; Stewart, M. P.; Bullock, R. M.; DuBois, M. R.; DuBois, D. L. *Science* **2011**, *333*, 863−866.
(34) Kilgore, U. J.; Roberts, J. A. S.; Pool, D. H.; Appel, A. M.; Stewart, M. P.; DuBois, M. R.; Dougherty, W. G.; Kassel, W. S.; Bullock, R. M.; DuBois, D. L. *J. Am. Chem. Soc.* **2011**, *133*, 5861−5872.
(35) Kilgore, U. J.; Stewart, M. P.; Helm, M. L.; Dougherty, W. G.; Kassel, W. S.; Dubois, M. R.; Dubois, D. L.; Bullock, R. M. *Inorg. Chem.* **2011**, *50*, 10908−10918.
(36) Wiese, S.; Kilgore, U. J.; Dubois, D. L.; Bullock, R. M. *ACS Catal.* **2012**, *2*, 720−727.
(37) Kütt, A.; Leito, I.; Kaljurand, I.; Sooväli, L.; Vlasov, V. M.; Yagupolskii, L. M.; Koppel, I. A. *J. Org. Chem.* **2006**, *71*, 2829−2838.
(38) Coetzee, J. F.; Kolthoff, I. M. *J. Am. Chem. Soc.* **1957**, *79*, 6110−6115.
(39) Thoi, V. S.; Karunadasa, H. I.; Surendranath, Y.; Long, J. R.; Chang, C. J. *Energy Environ. Sci.* **2012**, *5*, 7762−7770.
(40) McCrory, C. C. L.; Uyeda, C.; Peters, J. C. *J. Am. Chem. Soc.* **2012**, *134*, 3164−3170.
(41) Costentin, C.; Savéant, J.-M. *ChemElectroChem* **2014**, *1*, 1226−1236.
(42) Costentin, C.; Drouet, S.; Robert, M.; Savéant, J.-M. *J. Am. Chem. Soc.* **2012**, *134*, 11235−11242.

(43) Savéant, J.-M. *Chem. Rev.* **2008**, *108*, 2348−2378.
(44) Savéant, J.-M.; Su, K. B. *J. Electroanal. Chem.* **1984**, *171*, 341−349.
(45) Savéant, J.-M. *Elements of Molecular and Biomolecular Electrochemistry*; John Wiley & Sons, Inc.: Hoboken, NJ, 2006.
(46) Lexa, D.; Savéant, J.-M.; Schäfer, H. J.; Su, K.-B.; Vering, B.; Wang, D. L. *J. Am. Chem. Soc.* **1990**, *112*, 6162−6177.
(47) Stewart, M. P.; Ho, M.-K.; Wiese, S.; Lindstrom, M. L.; Thogerson, C. E.; Raugei, S.; Bullock, R. M.; Helm, M. L. *J. Am. Chem. Soc.* **2013**, *135*, 6033−6046.
(48) Daniele, S.; Ugo, P.; Mazzocchin, G.-A.; Bontempelli, G. *Anal. Chim. Acta* **1985**, *173*, 141−148.
(49) Kolthoff, I. M.; Thomas, F. G. *J. Phys. Chem.* **1965**, *69*, 3049−3058.
(50) Appel, A. M.; Helm, M. L. *ACS Catal.* **2014**, *4*, 630−633.
(51) Costentin, C.; Drouet, S.; Robert, M.; Saveant, J.-M. *Science* **2012**, *338*, 90−94.
(52) Sutin, N.; Creutz, C.; Fujita, E. *Comments Inorg. Chem.* **1997**, *19*, 67−92.
(53) Delahay, P.; Stiehl, G. L. *J. Am. Chem. Soc.* **1952**, *74*, 3500−3505.
(54) Schwarz, W. M.; Shain, I. *J. Phys. Chem.* **1965**, *69*, 30−40.
(55) Nicholson, R. S.; Shain, I. *Anal. Chem.* **1964**, *36*, 706−723.
(56) Savéant, J.-M.; Vianello, E. *Electrochim. Acta* **1965**, *10*, 905−920.
(57) Savéant, J.-M.; Vianello, E. *Electrochim. Acta* **1967**, *12*, 629−646.
(58) Andrieux, C. P.; Blocman, C.; Dumas-Bouchiat, J. M.; M'Halla, F.; Savéant, J.-M. *J. Electroanal. Chem.* **1980**, *113*, 19−40.
(59) Savéant, J.-M.; Su, K. B. *J. Electroanal. Chem.* **1985**, *196*, 1−22.
(60) Dempsey, J. L.; Winkler, J. R.; Gray, H. B. *J. Am. Chem. Soc.* **2010**, *132*, 16774−16776.
(61) Costentin, C.; Drouet, S.; Passard, G.; Robert, M.; Savéant, J.-M. *J. Am. Chem. Soc.* **2013**, *135*, 9023−9031.
(62) Hu, X.; Brunschwig, B. S.; Peters, J. C. *J. Am. Chem. Soc.* **2007**, *129*, 8988−8998.
(63) Dempsey, J. L.; Winkler, J. R.; Gray, H. B. *J. Am. Chem. Soc.* **2010**, *132*, 1060−1065.
(64) Solis, B. H.; Hammes-Schiffer, S. *Inorg. Chem.* **2011**, *50*, 11252−11262.
(65) Marinescu, S. C.; Winkler, J. R.; Gray, H. B. *Proc. Natl. Acad. Sci. U. S. A.* **2012**, *109*, 15127−15131.
(66) Felton, G. A. N.; Vannucci, A. K.; Chen, J.; Lockett, L. T.; Okumura, N.; Petro, B. J.; Zakai, U. I.; Evans, D. H.; Glass, R. S.; Lichtenberger, D. L. *J. Am. Chem. Soc.* **2007**, *129*, 12521−12530.
(67) Bhugun, I.; Lexa, D.; Savéant, J.-M. *J. Am. Chem. Soc.* **1996**, *118*, 3982−3983.
(68) Roubelakis, M. M.; Bediako, D. K.; Dogutan, D. K.; Nocera, D. G. *Energy Environ. Sci.* **2012**, *5*, 7737−7740.
(69) Quentel, F.; Gloaguen, F. *Electrochim. Acta* **2013**, *110*, 641−645.

dx.doi.org/10.1021/ic500658x | *Inorg. Chem.* 2014, 53, 9983−10002